Soft and Intelligent Reconfigurable Robotic Grasping

1st H.J.Keijts
Cognitve Robotics ME
Delft university of technology
Delft, The Netherlands
H.J.Keijts@student.tudelft.nl

***Abstract*—This paper presents a robotic grasping system that integrates soft robotic fingers, a reconfigurable gripper, and a YOLOv11-OBB-based object detection to enable intelligent adaptive, grasping. The system addresses the challenge of handling fragile and geometrically diverse objects—common in agricultural and food-handling applications—by dynamically adjusting its gripper configuration in response to object characteristics. A novel soft finger, selected through finite element modeling and experimental validation, provides compliant contact. The object detection model not only localizes and orients objects but also infers the optimal finger configuration, encoded via class ID. Experimental results demonstrate significant performance improvements: grasp success rates increased from 70% to 84,67% for fruits and from 66% to 84,67% for abstract objects, with only a modest 3-second increase in cycle time due to reconfiguration.**

***Index Terms*—soft robotics, grasping**

I. Introduction

Automation in agriculture and food handling is becoming increasingly important due to rising labor costs and seasonal labor shortages [1]. These industries involve manipulating fragile, irregularly shaped items such as fruits and vegetables, which pose significant challenges for traditional rigid robotic grippers [2]. For example, no two apples are exactly the same in size, shape, even within the same variety requiring grippers that can adapt to subtle differences.

The challenge extends beyond a single type of produce. In real-world settings, robots must handle a wide variety of items—ranging from soft fruits like tomatoes to firmer vegetables like cucumbers—within the same task. This demands a grasping solution that is both versatile and gentle. In addition to mechanical adaptability, food-handling tasks require delicate contact to prevent bruising or damage [3].

These factors make agriculture a particularly promising field for the application of soft robotics. Soft, compliant grippers can conform to the shape of diverse objects and reduce the risk of damage. For example, Visentin et al. [4] presented a pneumatically actuated soft gripper optimized for gentle and conformal contact with fruit. Similarly, Gafer et al. [5] proposed a quad-fingered soft gripper for harvesting, and Morikage et al. [6] developed a multi-modal gripper that adapts to produce of varying sizes and rigidity. In addition, Elfferich et al. [7] designed a soft robotic gripper specifically tailored for harvesting blackberries, utilizing a compliant structure to minimize damage during grasping.

However, relying solely on soft fingers may not be sufficient when dealing with the full range of objects encountered in agricultural settings. To address this, researchers have begun exploring reconfigurable grippers, which can change their geometry or structure based on the task. Baggetta et al. [8] introduced a modular gripper capable of adjusting its configuration to handle different fruits and vegetables. Other reconfigurable systems have been proposed by Cheng et al. [9] and Hashanjana et al. [10].

Hybrid approaches that combine soft robotics with reconfigurable mechanisms are promising. Mishra et al. [11] introduced SIMBA, a biologically inspired system integrating modular soft fingers with mechanical reconfiguration. Similarly, Khin et al. [12] proposed a hyper-redundant gripper system for enhanced adaptability. Recent systems like RESoft [13] and the food-handling soft robot by Mathew et al. [14] demonstrate the growing interest in these hybrid designs.

Meanwhile, advances in computer vision—particularly object detection models like YOLO—have enabled robust detection, in agricultural robotics [15]–[18]. Despite these developments, few robotic systems fully integrate *soft fingers*, *reconfigurable grippers*, and *vision-based perception* into a cohesive, autonomous platform.

a) Research Gap and Objective: While soft and reconfigurable grippers have independently shown great promise in agricultural and food-handling contexts, there remains a critical gap in integrating these technologies with perception in a unified system. Most existing approaches treat softness, reconfigurability, and vision as separate components rather than parts of a coordinated design.

This work aims to address that gap by investigating the integration of soft robotic fingers and a reconfigurable gripper, controlled by a perception-driven adaption. Specifically, it seeks to answer the following research question:

> *How can soft fingers and a reconfigurable gripper be combined within a robotic system to detect and grasp a variety of objects?*

Experimental results demonstrate that the proposed system achieves higher grasp success rates compared to fixed-configuration grippers, particularly when handling objects with

varying shapes and surface characteristics.Experimental results demonstrate that the proposed system achieves higher grasp success rates compared to fixed-configuration grippers, the success rate for grasping fruits increased from 20 out of 30 to 25 out of 30 attempts, while for abstract shapes, it improved from 19 out of 30 to 24 out of 30. This performance gain comes with a modest increase in cycle time, from 53 seconds to 57 seconds

II. METHODOLGY

This methodology is divided into three main sections. First, the system design is presented, detailing the integration of the robotic arm, reconfigurable gripper, control architecture, and motion planning pipeline. Second, the soft finger design and selection process is described, Finally, the third section covers YOLO training and adaptation, outlining the dataset preparation, model tuning for object detection with oriented bounding boxes, and evaluation of detection performance.

A. System Design

This section outlines the design of the robotic system used for grasping various objects. It outlines the hardware and software architecture, task objectives, and design criteria.

1) Task Definition: The objective of the robotic system is to autonomously detect and grasp a variety of items—particularly delicate objects such as fruits. This task demands a combination of adaptable gripping, soft fingers, control, and robust visual perception. This is important as robotic systems aim to be generalizable and adaptable to variations in object shape and size.

2) System Overview:

a) Existing Hardware: The system uses the Franka Emika Panda robotic arm. Mounted at the end-effector is a reconfigurable robotic gripper, available in Philab. An Intel RealSense camera is mounted on the robotic arm to provide image stream data for visual perception. In figure 1 the physical robots is shown.

b) Novel Contributions: This work contributes several innovations to the existing hardware. First, soft fingers have been designed for intergration with the reconfigurable gripper to enable compliant and adaptable grasping. Second, the YOLOv11-OBB (Oriented Bounding Box) object detection algorithm has been adapted to inform the system on the desired gripper configurations. Finally, the system has been fully integrated into a complete and functional robotic system that combines perception, control, and actuation. This includes the electrical design, software architecture (ROS2), and the finite state machine (FSM) governing the system's operation.

3) Criteria: To find the design criteria, from a real-world perspective, it is good to start with more general non-technical requirements such as economic output. In this case, the goal is to maximize economic output, defined as:

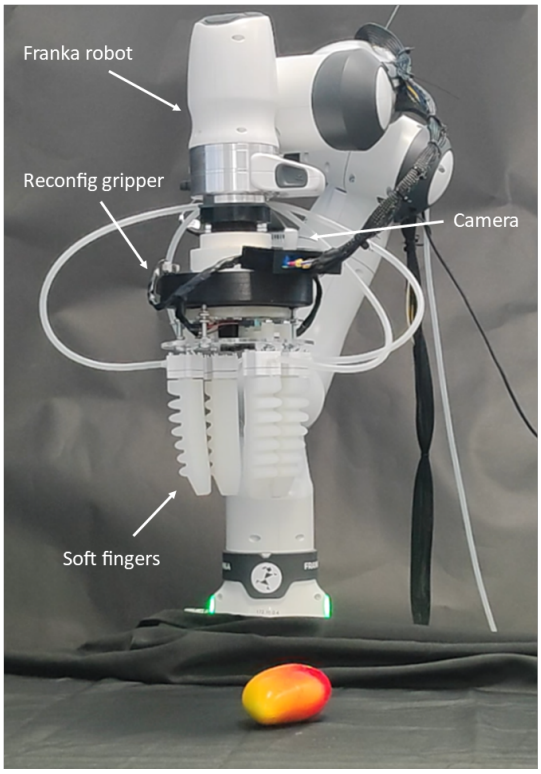

Fig. 1: The robotic system, highlighting key hardware components including the soft fingers and reconfigurable gripper

$$\text{Economic Output} = \text{Production Output} - \text{Total Cost} \quad (1)$$

Production output is defined as:

$$\text{Production Output} = Q \times T \quad (2)$$

where Q is the successful task rate (grasps per unit time), and T is the total system uptime.

a) Costs: Total cost is the sum of all operational and setup expenditures:

$$\text{Total Cost} = C_{\text{robot}} + C_{\text{supervision}} + C_{\text{damage}} + C_{\text{maintenance}} + C_{\text{energy}} \quad (3)$$

- **Robot Cost** (C_{robot}): Includes both hardware and software components—robot arm, reconfigurable gripper, sensors, controllers, ROS2 integration, YOLOv11 object detection, and FSM logic.
- **Supervision Cost** ($C_{\text{supervision}}$): Human involvement for monitoring or intervention.
- **Damage Cost** (C_{damage}): Costs due to product damage, especially with fragile items.
- **Maintenance Cost** ($C_{\text{maintenance}}$): Part replacement and cost of downtime.
- **Energy Cost** (C_{energy}): Power usage of all subsystems during operation.

b) Design Criteria: The costs as well as the output result in the following design criteria:

- **Autonomy**: Achieved through tight integration of perception, planning, and actuation. Reduces $C_{\text{supervision}}$ and downtime costs.
- **Speed**: Enabled by real-time processing (YOLOv11-OBB, fast FSM transitions, and low-latency actuation), which increases Q in the production output.
- **Adaptability**: Facilitated by the reconfigurable gripper and soft fingers, allowing grasping of a variety of shapes and sizes with minimal delay.
- **Non-intrusiveness**: Designed with soft fingers to avoid damaging the objects.

The following sections outline the system architecture, detailing the integration of hardware and software components, including the reconfigurable gripper, perception, motion planning, soft actuation, and control via a finite state machine. A wiring and network overview is also provided.

4) Reconfigurability and Control: The gripper is mechanically reconfigurable, allowing changes in finger layout depending on object geometry. Although the gripper always uses four fingers for grasping, it can be configured in 2-, 3-, or 4-finger as layouts different grasp strategies, see Figure 2 for configurations. The total finger-to-finger width of the gripper is 150 mm.The mass including soft fingers is 1.29 kg

This gripper already exists as a hardware prototype. For this work, development of the the electrical wiring and control logic, using a Raspberry Pi 4B was done. The system includes four end-position switches to detect the current gripper configuration. It operates under ROS2, continuously publishing the current configuration and subscribing to a desired goal configuration. A DC motor actuates the gripper to transition to the target configuration. Wiring schematics and logical diagrams are provided in the appendix C.

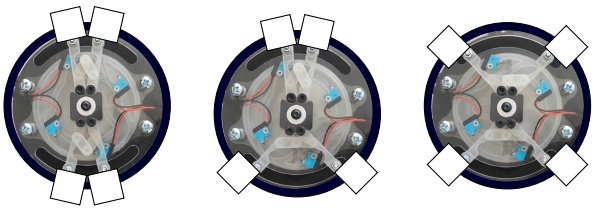

(a) 2-finger configuration (b) 3-finger configuration (c) 4-finger configuration

Fig. 2: Schematic illustration of the different finger configurations enabled by the reconfigurable gripper design.

5) Panda Motion Planning: Motion planning for the Franka Emika Panda arm is implemented using key-point interpolation. The robot moves between predefined waypoints. Collision checking is performed at each interpolation step to ensure safe motion within the environment and avoid collisions with the workspace, or the robot itself.

6) Perception and Object Detection: YOLOv11-OBB is employed for real-time object detection. The algorithm processes camera input from the Intel RealSense camera and outputs oriented bounding boxes along with class IDs.

7) Soft Finger Selection: A aspect of the system's adaptability is the integration of soft fingers, which enable compliant and safe interaction with fragile or irregularly shaped objects. The soft fingers are pneumatically actuated and controlled via Festo VTEM valves.

8) Finite State Machine: The robot's control architecture is implemented using a Finite State Machine (FSM), which governs high-level task execution see Figure 3 or see appendix A for an enlarged diagram.

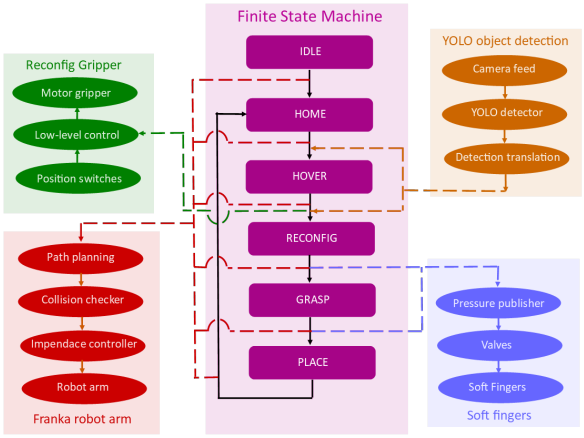

Fig. 3: Diagram of the Finite State Machine and its interactions with other components compiling the robotic system

The FSM follows these states:

1) **Idle** – The system initializes and waits for a command. Upon activation, the robot moves to the home position using the Franka Emika Panda arm.
2) **Home** – The robot moves to a predefined home position with the camera pointing straight down. It then processes input from the YOLO model to identify and locate objects.
3) **Hover** – The robot selects the nearest object based on YOLOv11-OBB output for time-efficient execution. It then moves the end-effector above the selected object using the Panda arm.
4) **Reconfigure** – Based on the object's orientation and class from YOLO detection, the gripper configuration is adjusted accordingly. This involves actuating the gripper reconfiguration mechanism and aligning the Z-axis orientation using the Panda arm.

5) **Grasp** – The robot lowers the gripper to the object. Soft fingers are actuated using VTEM valves to execute the grasp.
6) **Place** – The robot lifts the object and transports it to a predefined placement location. The Panda arm moves, and the object is released using the VTEM valves. After placing the object, the robot returns to the home position to begin a new cycle.

9) Physical Wiring Overview: Figure 26 in the appendix B shows the system's physical wiring and network architecture. The RealSense camera connects via USB-Serial to the main laptop (172.16.0.7), which runs YOLOv11-OBB, the Finite State Machine (FSM), and a ROS1–ROS2 bridge. The Panda robot arm (172.16.0.4) and its controller (172.16.0.1) operate under ROS1 and are connected via LAN 1.

VTEM valve control runs on a dedicated PC (172.16.0.15) with ROS2 and communicates with the valves over Modbus and via LAN 2. The reconfigurable gripper is controlled by a Raspberry Pi (172.16.0.10) running ROS2, connected via a 5V digital signal. All components are integrated through a combination of ROS1 and ROS2 nodes, bridged at the central laptop.

B. Soft finger design and selection

This section covers soft finger design, developed, selection, and validation. The soft finger was designed as a pneumatic actuator due to its fast response time, cost-effectiveness, and the availability of pneumatic infrastructure in industrial settings. Pneumatic bellow actuation enables large bending angles [19], supports rapid movement compared to traditional PneuNet structures [20], and offers a low-cost solution [21] with fast actuation and high force to pressure ratio [22].

1) Design: The pneumatic actuator as can be seen in figure 4; comprises a soft finger made from a single piece of silicone rubber and a two-part back connector. The back connector serves dual purposes: it enables mounting the soft finger onto a robotic gripper and provides a port for attaching the pneumatic tubing.

a) Fingerbody design: The soft finger features a multi-chamber geometry constructed from silicone rubber. It includes six internal chambers that enable bending when pressurized. The bottom layer of the finger incorporates a friction-enhancing structure and acts as a strain-limiting layer. This layer converts the extension caused by the inflation of the air chambers into bending motion. To support this function, the bottom layer is made from a stiffer silicone and is thicker compared to the top layer. In the design shown in Figure 4b, the chamber walls are 3 mm thick, while the bottom layer has a thickness of 5 mm as can be seen in figure 4b. The finger has a mass of 68 grams and an effective length of 115 mm a width 25 mm. The working pressure is 35 kPa. In figure 4b. all dimension in figure are in millimeters

b) Fingertip design: At the fingertip, a nail-like structure is integrated into the design to enhance the finger's tactile reach. Additionally, the sides of the fingertip are slightly pointed inward, see figure 4a, to prevent collision between adjacent fingers during gripping tasks, thereby improving the range of object sizes and shapes that can be grasped.

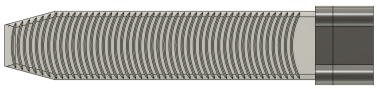

(a) Bottom view of the soft finger, showing surface features.

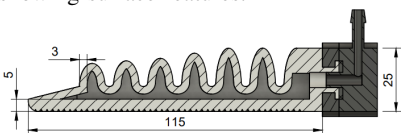

(b) Internal structure of the soft finger, highlighting the chamber layout

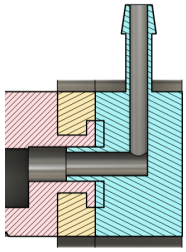

(c) Cross-sectional view of the connector design

Fig. 4: Detailed views of the soft finger design, including external geometry, internal chamber structure, and connection interface.

c) Fingerbottom design: To increase grip performance, the bottom surface incorporates a patterned friction layer consisting of 0.8 mm deep grooves with an v-shaped profile along an arced path. This structure enhances contact stability through increased surface friction and helps prevent slippage during object manipulation. The work of [23] demonstrated that a patterned friction layer can significantly improve the grip of a soft robotic fingers.

d) Finger-connector design: The back connector consists of two parts, as shown in Figure 4c: the yellow ring with a blue block. The ring and block together form the back connector. The blue block connects to the gripper, while pneumatic tubing is attached to a hose barb.

The soft silicone finger(pink) fits through the yellow ring, due to the finger's elasticity, and flares out beyond it. This flaring, combined with the extension past the ring, enables a shape-locking mechanism when the block is connected. As the block is connected, a cylindrical extension on its inner side pushes inward into the finger, securing it in place. Simultaneously, the flared portion of the finger is compressed between the ring and the block, creating an airtight seal.

This assembly achieves both an airtight seal and a shape-locked connection, using only the two components by integrating multiple functions into on part.

e) Geometric variants: Three geometric variants of the soft finger were developed, see figure 5, each tailored to produce distinct displacement profiles.

The Geometric variants are:

- **FH-models**: Feature smaller chambers positioned higher up along the finger, away from the fingertip, designed to concentrate bending near the tip.
- **FN-models**: Include chambers of uniform size distributed evenly along the finger length, resulting in a circular bending profile.

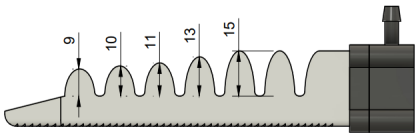

(a) FL model

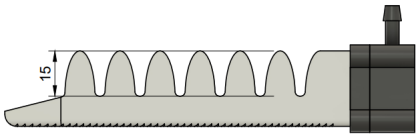

(b) FN model

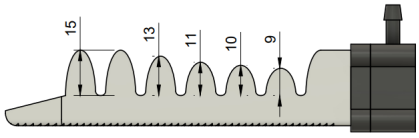

(c) FH model

Fig. 5: Variants of the soft finger design—FL, FN, and FH

- **FL-models**: Incorporate smaller chambers located closer to the base, promoting bending near the mounting point.

The designs are illustrated in Figures 4 and 5, showing the chamber layout, fingertip profile, and friction pattern details. more detailed drawings can be found in appendix D.

2) Selection: To select the design of the soft finger, finite element method (FEM) analysis was conducted using COMSOL Multiphysics. The soft material behavior was modeled using the Yeoh hyperelastic model derived from [24].

The Yeoh model constants used were:

- Dragon Skin 20: $C_{10} = 0.1361$, $C_{20} = 0.0009$, $C_{30} = 0$
- Dragon Skin 30: $C_{10} = 0.0709$, $C_{20} = -0.01015$, $C_{30} = 0.0002$

Using FEM simulations, the touchable range and output force were determined for different finger geometries.

a) Touchable Range Estimation: A theoretical evaluation using FEM was conducted to determine the feasible range of cylindrical objects that can be contacted by a two-finger soft robotic gripper.

Assuming the gripper, see Figure 6, consists of two soft fingers (gray) mounted 150 mm apart, inside to inside finger, on a rigid base (red), oriented directly opposite one another. The objects considered are upright cylinders (green) placed on a flat ground plane (blue), centered between the fingers. The goal is to determine the maximum range of cylinder dimensions defined by height h and radius r that can be contacted by the finger tips without any part of the fingers or gripper colliding with the ground.

Two grasping strategies were simulated:

1) *Sequential Actuation Test*: The gripper is first positioned vertically above the object and lowered to a target height. After reaching this height, the fingers are actuated from an initial vertical (non-bending) state into their final curved grasping shape.
2) Simultaneous Actuation Test: The gripper descends vertically while the fingers bend simultaneously, following any ideal actuation profile. The gripper's motion remains strictly vertical throughout.

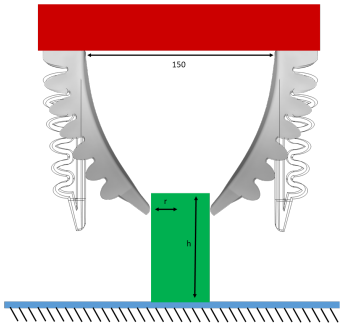

Fig. 6: Diagram of assumed scenario for analyses touchable range of the soft finger.

Figures 7a and 7b show the resulting touchable regions under both actuation strategies, 3 dimensional version of these plots can be found in Appendix H. The FL model demonstrates a greater touchable range in both cases.

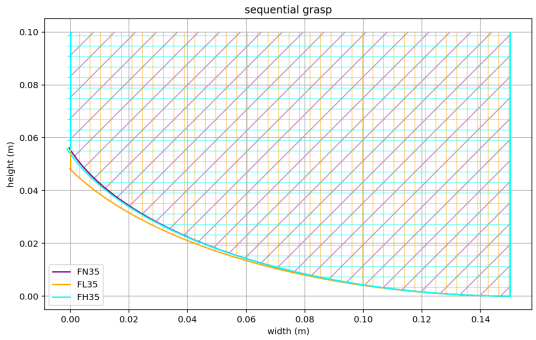

(a) Touchable range for the sequential actuation scenario.

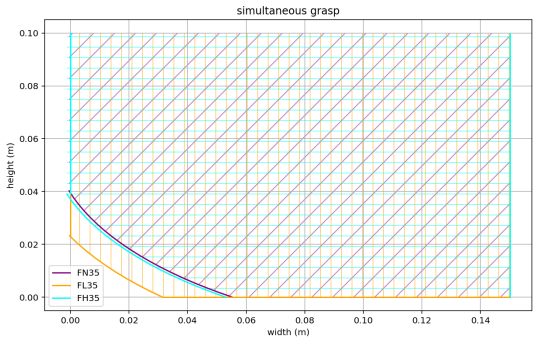

(b) Touchable range for the simultaneous actuation scenario.

Fig. 7: Comparison of the soft finger's touchable range for sequential and simultaneous actuation scenarios for three different model variants.

In the sequential actuation scenario, the motion concentrated near the base leads to a more favorable ratio of inward motion

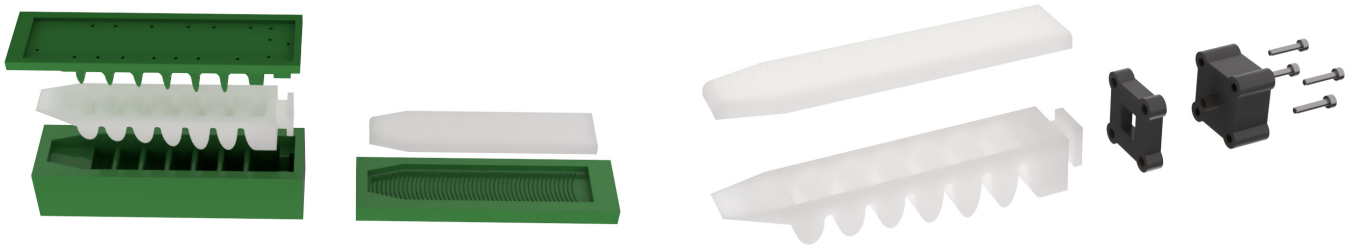

(a) Molding process soft fingers

(b) exploded view assembly soft fingers

Fig. 8: Fabrication steps of soft fingers

to upward displacement. This allows the fingertip to move more inward, rather than lifting away from the object.

In the simultaneous actuation case, the smaller bellows near the fingertip prevent collisions between the air chambers and the ground as the finger bends and the gripper moves downward.

These effects is especially pronounced during simultaneous actuation, where FL models are capable of touching cylinders with smaller radii this leads to the selection of the FL-models for the soft fingers.

Nonetheless, grasping objects with both small radius and low height remains challenging. In such cases, the fingers may either move above the object without making contact or collide with the bellows before the fingertip reaches the target.

b) Force Output and Wall Thickness Effects: Modifying the wall thickness of the finger geometry has a impact on the output force at the fingertip. Thinner walls result in higher force generation under the same internal pressure due to reduced stiffness. However, this increased force comes at the expense of structural integrity. Thinner walls are more prone to failure and fatigue, and they also exhibit greater passive compliance. This can result in undesired "jiggling" and misalignment during grasping tasks.

Figure 9 shows force output versus pressure for several FL model variants: FL24, FL35, and FL46, corresponding to wall thicknesses of 2 mm, 3 mm, and 4 mm, respectively. The strain-limiting layer for each was 4 mm, 5 mm, and 6 mm.

It is important to note that while thinner walls offer a higher force-to-pressure ratio, they also result in a larger bending-angle-to-pressure ratio. Therefore, although thicker-walled fingers may be less force-efficient at a fixed pressure, they can produce greater force at the same bending angle.

Taking these trade-offs into account, the FL35 model—with 3 mm wall thickness and a 5 mm strain-limiting layer—was selected as the final design. This configuration offers

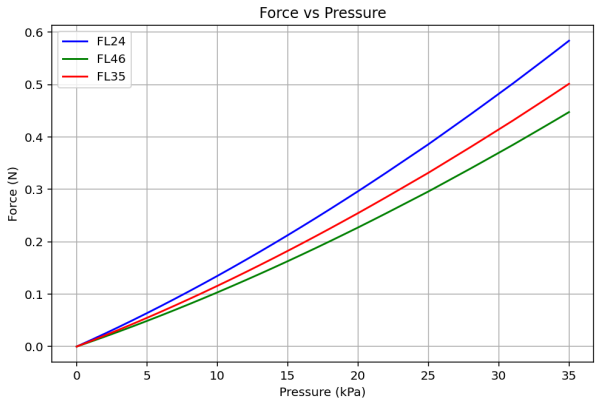

Fig. 9: Force output versus pressure for different wall thicknesses (all FL models).

a balanced compromise between force output, bending performance, and structural integrity.

3) Fabrication: The soft fingers were fabricated using a multi-step molding process. The molds were 3D-printed in PLA. A three-part mold was used for the top layer, consisting of two printed mold halves and an M6 bolt used to form the internal airway of the finger. The bottom layer was cast using a single-part mold, see figure 10a.

The top layer was cast from Dragon Skin 20, and the bottom layer from Dragon Skin 30. Both were degassed in a vacuum chamber to remove air bubbles, then cured fully inside their molds. After curing, the layers were bonded together using Dragon Skin 20 as an adhesive.

The back connector of the finger was also 3D printed in PLA and included M3 threaded inserts. Following is the assembly, the soft finger was inserted trough the ring and fastened to the block using four m3 bolts as can be seen

in figure 8b. More detailed drawing can be found in the appendix D.

4) Experiments: To validate the accuracy of the FEM model, experiments were conducted using three soft finger variants: FL35, FN35, and FH35. The FL35 variant was selected for integration into the robotic system, and its experimental results are presented in Figure 10. Results for FN35 and FH35 are provided in Appendices F and G. and the experimental setups are detailed in Appendix E.

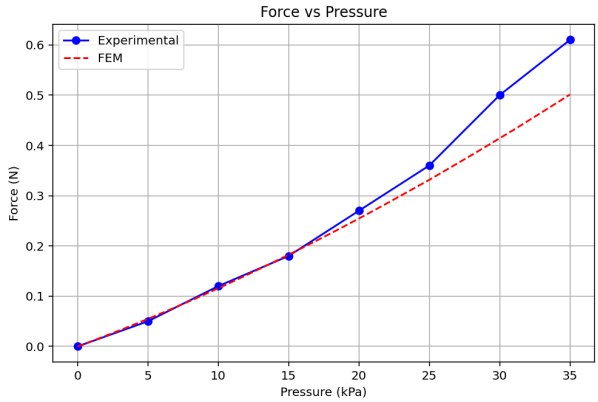

(a) Force comparison between the FL35 FEM model and experimental results.

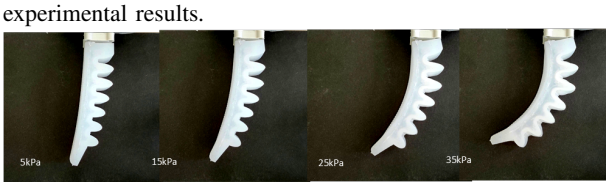

(b) Observed bending motion of the FL35 finger during the experiment.

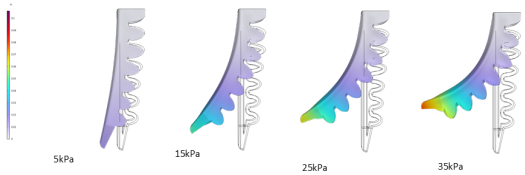

(c) Simulated bending behavior of the FL35 finger using the FEM model.

Fig. 10: Validation of the FL35 soft finger design through experimental measurements and FEM simulations.

a) Force and Motion Validation: Two types of validation experiments were carried out; output force measurement and bending motion comparison. The experimental setup for force testing involved clamping the soft finger and actuating it while a force sensor recorded the reaction force, see appendix E for setup. As shown in Figure 10a, the measured output force is generally higher than the FEM predictions, especially at higher pressures. This discrepancy is likely due to nonlinear material behavior not fully captured in the FEM simulation.

For motion analysis, Figures 10b and 10c compare the experimental and simulated bending motions. The FEM model predicts slightly greater bending than observed in the experiments. This difference may result from fabrication imperfections or unmodeled nonlinearities in the material properties. Despite these deviations, the overall deformation trends are consistent across all finger variants. This suggests the FEM model remains a valid tool for design selection.

b) Friction Characterization: An experiment was conducted to quantify the friction coefficient using the Coulomb friction model as an approximation of performance. In each test, the angle of inclination was gradually increased until the finger began to slide, allowing for the measurement of static friction coefficients. The coefficients were calculated from the critical angles using the relation $\mu = \tan(\theta)$. See Appendix F for details of the experimental setup and a free body diagram of the setup.

Tests were performed on the following materials:

- **Wood:** A rough, coarse, and irregular surface ($R_a \approx 5$–$10\ \mu$m).
- **PVC:** Matte finish, moderately smooth ($R_a \approx 3.0\ \mu$m).
- **Mild Steel (AISI 1018):** Brushed finish, uniform and smooth surface ($R_a \approx 0.8\ \mu$m).

Each material was tested using both untextured and textured versions of the soft finger. The results, presented in figure 11, show that texturing the finger generally increases friction, particularly on Wood and PVC. This indicates that surface patterning can be a useful strategy for enhancing grip.

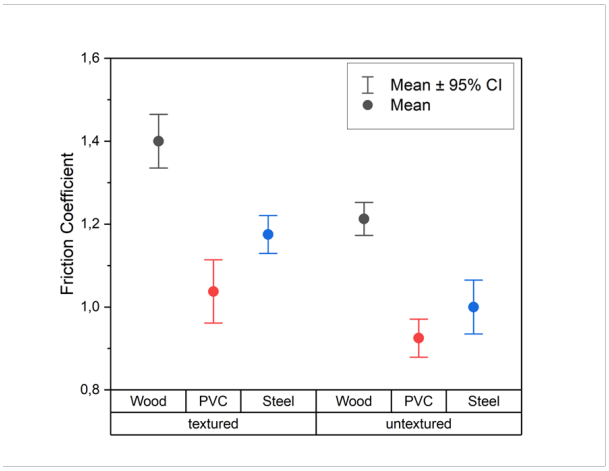

Fig. 11: Friction coefficients for different materials using untextured and textured soft fingers.

C. YOLOv11-OBB Selection and Evaluation

This section presents the rationale behind selecting the YOLOv11-OBB object detection model and details its implementation, training, and evaluation for grasp detection.

YOLOv11-OBB was selected over alternative object detection algorithms due to its high inference speed, support for oriented bounding boxes (OBBs), and robustness when trained on small datasets [25]. The angle-aware detection enabled by OBBs allows the robotic system to adjust its gripper vertical axis rotation, aiming to improve manipulation success rates. Additionally, the detection class ID was

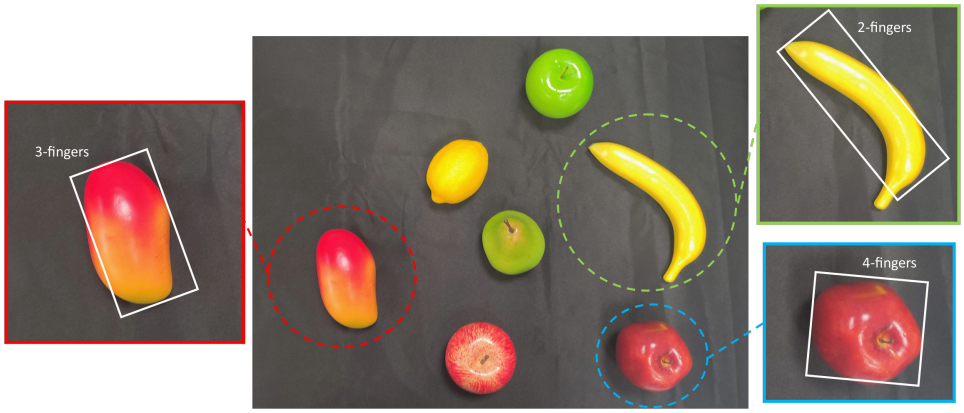

Fig. 12: Illustrative example of object detection used to guide the grasping.

repurposed to encode the gripper configuration, specifying whether a two-, three-, or four-finger grasp should be applied.

1) System Functionality: The system utilizes YOLOv11-OBB to perform three simultaneous tasks:

- Object Localization – Detects object position in the image.
- Orientation Estimation – Uses OBBs to predict the object's rotation.
- Grasp Configuration Classification – Encodes the required gripper type (two-, three-, or four-finger) directly as the detection class ID.

This allows the robot to determine where to grasp an object, how to orient its gripper by rotation around its vertical axis, and which gripper configuration to use. For an illustrative example of detection for grasping see figure 12

2) Model Variants and Input Modalities: To explore the trade-offs between inference speed, detection accuracy, and generalization, four variants of the YOLOv11-OBB model were developed and tested. These included both small and nano versions of the model, each trained in grayscale and color formats. The grayscale models were evaluated to determine whether reducing input channel dimensionality could maintain sufficient accuracy while lowering computational load. Moreover, it was hypothesized that grayscale inputs could improve generalization in low-data regimes by reducing color-specific noise and encouraging the model to focus on structural features such as shape and contrast. In contrast, the color models were expected to leverage richer features, which could lead to superior performance when a larger dataset is available.

3) Dataset and Preprocessing: Training was performed using a custom dataset consisting of 334 images representing 150 distinct object instances, with illustrative examples provided in the appendix I. Each object was placed against a uniform black background. The preprocessing steps included resizing to 640×640 pixels using an envelope resizing approach that preserved the original aspect ratios; this is import as the aspect ratio of the object influences the desired gripper configuration. For the grayscale model variants, images were converted from RGB to grayscale prior to training. The dataset was divided into training, validation, and test subsets, and all models were trained for 100 epochs using the default YOLOv11 training configuration.

4) Data Augmentation: To enhance model robustness and generalization, data augmentation was applied during training. Each original image was used to generate three augmented variants applying controlled variations in hue and brightness, with hue adjusted by ±15 degrees and brightness modified by ±15%. These enhancements were designed to simulate visual variability in real-world conditions, aiming to improve the model's ability to robust against sensor imperfection and varying lightning conditions.

5) Evaluation Protocol: The system was evaluated using two separate test datasets, both containing images that were not used during training. The first dataset, referred to throughout this paper as the seen object dataset, includes 32 images featuring previously encountered object categories placed in novel positions and orientations. The second dataset, referred to as the unseen object dataset, consists of 32 images containing entirely new objects not present during training. This setup enables a direct assessment of the model's ability to generalize to both familiar and unfamiliar scenarios. Examples from both datasets can be found in the Appendix I.

6) Evaluation Results: The following figures provide a detailed summary of the performance of the YOLOv11-OBB model variants across a range of evaluation metrics. Figures 13a and 13b present the mean average precision (mAP) scores at multiple Intersection over Union (IoU) thresholds for the seen and unseen object datasets, respectively. Confusion matrices are shown in Figures 14b and 14c, which illustrate the model's classification performance on the seen and unseen datasets, respectively. These matrices are generated using a confidence threshold of 0.25. The confusion matrix in Figure 14a shows the classification results on the training set.

Precision–recall curve plots for all model variants, across both datasets and all class IDs, can be found in Appendix J.

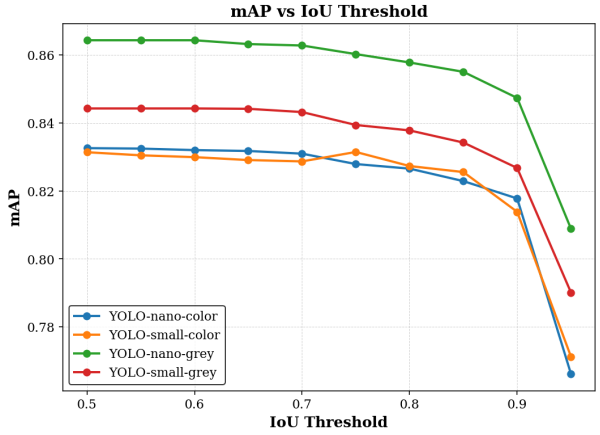

(a) Mean Average Precision (mAP) at various IoU thresholds for unseen images of previously seen objects.

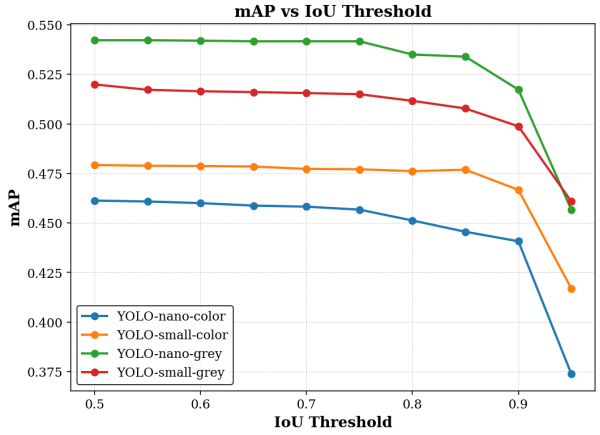

(b) Mean Average Precision (mAP) at various IoU thresholds for unseen images of previously unseen objects.

Fig. 13: Comparison of mean Average Precision (mAP) across Intersection over Union (IoU) thresholds for two generalization scenarios: (a) unseen images of previously seen objects and (b) unseen images of previously unseen objects.

The mAP plots in Figures 13a and 13b show that the YOLOv11-nano grayscale model consistently outperforms the other model variants across all IoU thresholds on both the seen and unseen object datasets. This superior performance may be attributed to the model's smaller architecture, which tends to generalize better on limited datasets due to a reduced risk of overfitting. Additionally, the use of grayscale input likely encourages the model to focus more on structural and geometric features rather than color. These characteristics together appear to enable stronger generalization.

Notably, the performance gap between the YOLOv11-nano grayscale model and other variants is more pronounced on the unseen object dataset. This suggests that the grayscale nano model not only generalizes better to unseen images but is also more effective at adapting to entirely new objects. One possible explanation is that the unseen objects, often share structural similarities with seen objects. By focusing on shape and contour rather than texture or color, the model is able to extract more domain-invariant features, resulting in stronger generalization to previously unseen objects.

Interestingly, the mAP curves remain relatively consistent across a wide range of IoU thresholds, with only a noticeable decline beyond an IoU of 0.9. This suggests that the models are capable of achieving good localization and orientation predictions. One possible reason for this is that while the model's bounding box predictions are spatially accurate, it struggles more with assigning the correct class labels.

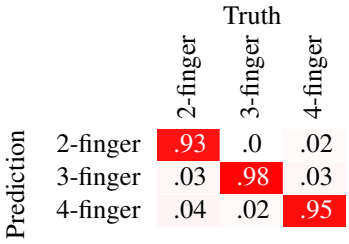

(a) Confusion matrix training of YOLO-nano-grey

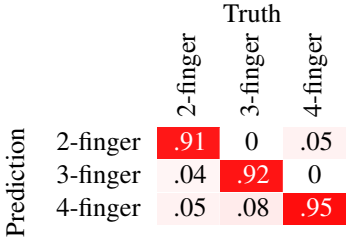

(b) Confusion matrix testing of YOLO-nano-grey for seen objects unseen images

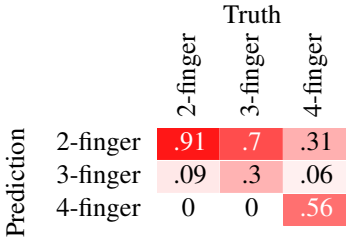

(c) Confusion matrix testing of YOLO-nano-grey for unseen objects

Fig. 14: Confusion matrices showing YOLO-nano-grey performance across different evaluation scenarios: (a) training, (b) test on unseen images of known objects, and (c) test on unseen objects.

This observation is further supported by the confusion matrices. In the case of the seen object dataset, the confusion matrix shows reasonably good classification performance, with most classes being correctly identified. However, for the unseen object dataset, the classification performance degrades more significantly. This is especially evident for certain object types such as the 3-finger gripper configuration, which the model frequently misclassified. This indicates that the model has difficulty generalizing class identity for previously unseen object shapes, even if it can reasonably detect their presence and location. From the confusion matrix on the training set, it can be seen that the model is not overfitting to the

training images, as the classification performance remains strong. However, when compared to the confusion matrix on completely unseen images, the model appears to be overfitted or, at the very least, struggles to generalize to novel object shapes.

To assess the computational efficiency of the different YOLOv11-OBB variants, the number of floating-point operations (FLOPs) was estimated. YOLOv11-nano models both grayscale and RGB require 3.35 GFLOPs per inference, while the YOLOv11-small models require 11.27 GFLOPs. These estimates correspond to single-image inference at a standard resolution of 640×640 pixels.

III. RESULTS

This section presents the evaluation of the robotic system's grasping performance across different finger configurations, including fixed 2-, 3-, and 4-finger setups, as well as the proposed reconfigurable setup capable of dynamically adjusting its finger layout. The study investigates the effectiveness of combining soft fingers with a reconfigurable gripper in a robotic system designed to detect and grasp various object. The objective is to determine whether dynamically adjusting the finger configuration improves grasp success compared to fixed finger setups across various objects.

1) Experimental Setup: The robotic system, described in Section II-A, is tested using three artificial fruits—a banana, a mango, and an apple. which can be see in figure 16a, 16b and 16c respectively.

(a) Banana (b) Mango (c) Apple

Fig. 16: Top view of artificial fruits (banana, mango, and apple) used for evaluating the robotic system.

The fruits are placed within the robot's visible workspace, measuring approximately 60 cm × 45 cm. Each fruit was positioned inside a basket of approximately 25 cm × 15 cm, located 80 cm right from the workspace center. A black fabric was used as a background. Lighting conditions simulated typical indoor environments, combining ambient and consistent artificial light to ensure repeatability. In figure 1 the setup can be seen.

For comparison, grasps were attempted using fixed configurations that did not adapt. For each object, fixed 2-, 3-, and 4-finger setups were used. Additionally, all objects were tested using the proposed robotic system, which reconfigures based on the YOLO-proposed configuration. The reconfigurable gripper adjusted its finger layout to match the selected configuration.

Each configuration was tested with 100 grasp attempts per object. A grasp was considered successful if the object was successfully placed into the basket. Figure 15 presents the results, showing percentage os successful grasp for each fruit and configuration as well as the 95% confidence interval. Additionally, Figures 17, 18, and 19 show examples of successful and failed grasps for 2-, 3-, and 4-finger configurations, respectively.

2) Abstract Shapes: To evaluate generalization beyond natural object shapes, the system was also tested on three abstract objects made from Duplo blocks (see Figure 21). These objects will henceforth be referred to as Object A, Object B, and Object C. Each was designed to be preferred a specific grasp configuration—2-finger, 3-finger, and 4-finger, respectively.

Each of these shapes was selected to assess the grasping system's adaptability to non-fruit, structurally diverse objects. As with the fruit trials, each configuration underwent 100 grasp attempts per object.

Figure 20 summarizes the grasp success rates for the abstract objects under different finger configurations. Additionally, Figures 22, 23, and 24 illustrate examples of both successful and failed grasp attempts for 2-, 3-, and 4-finger configurations, respectively.

To assess the increase in cycle time which important in relation to cost. The time for a single cycle is 37 seconds on average, of which 3 seconds are spent on gripper reconfiguration.

IV. DISCUSION

The experimental evaluation highlights the beneficial effects of automatic reconfiguration on robotic grasping performance. Addressing the question of whether combining soft fingers with a dynamically reconfigurable gripper enhances grasp success across varied objects. Across both natural (fruit) and abstract objects, the results demonstrate that the adaptability provided by the reconfigurable gripper significantly improves overall grasp success.

A. Effect of Reconfiguration on Grasp Performance

To address the question of whether dynamically adjusting the finger configuration enhances grasp success compared to fixed setups, the grasping performance was evaluated on natural objects with various finger configurations. For natural objects, grasp success varied noticeably depending on object shape and finger configuration. As shown in Figure 15, fixed configurations produced inconsistent results. For example, the 2-finger setup achieved high success with the banana due to its elongated shape but struggled with rounder objects like the apple. Meanwhile, the 3-finger and 4-finger configurations succeeded with rounder objects but were less effective with the banana. Interestingly, the banana proved more difficult to grasp overall, yet using the 2-finger configuration notably improved its success rate.

In contrast, the reconfigurable setup outperformed the fixed configurations by dynamically adjusting its finger layout to suit the object. This adaptability led to more stable grasps. The YOLO-based configuration selection plays a key role

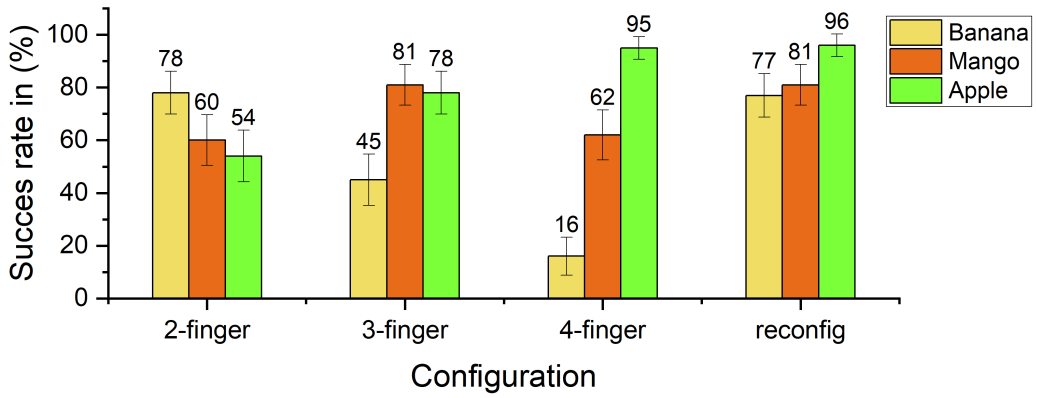

Fig. 15: Grasp success rates for different fruits using various finger configurations. Each bar shows the percentage of successful grasps out of 100 trials with 95% confidence intervals.

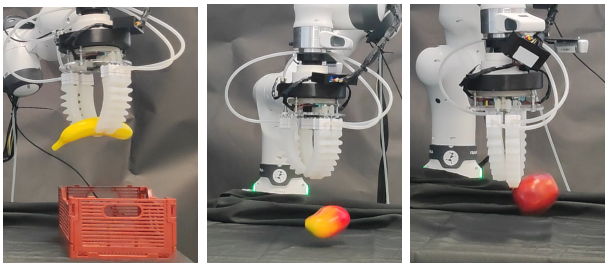

(a) Banana successful grasp (b) Mango failed grasp (c) Apple failed grasp

Fig. 17: Examples of 2-finger grasp attempts on different fruits: one successful and two failed grasps.

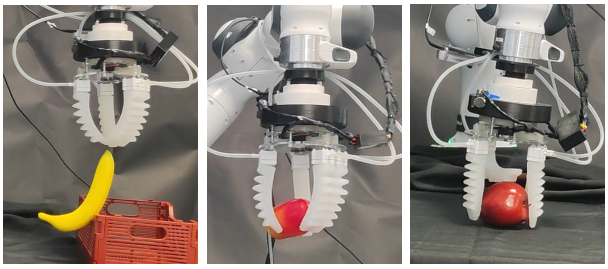

(a) Banana failed grasp (b) Mango successful grasp (c) Apple failed grasp

Fig. 18: Examples of 3-finger grasp attempts on different fruits: one successful and two failed grasps.

by recommending the most suitable finger layout for each object. While the system's grasp success did not always reach the theoretical maximum (where the best configuration is perfectly selected every time), it remained close. Occasional misclassifications by the object detector slightly reduced performance, but these errors more often occurred with ambiguous shapes—cases where the alternative configuration still yielded a reasonably high success rate. For example it was more common 3 finger was selected wrongly for apple than 4 finger for banana

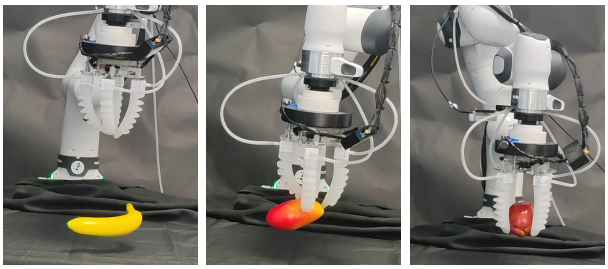

(a) Banana failed grasp (b) Mango failed grasp (c) Apple successful grasp

Fig. 19: Examples of 4-finger grasp attempts on different fruits: one successful and two failed grasps.

Grasping performance improved significantly with the adaptive system, reaching 84.33% for abstract objects and 84.67% for fruit, compared to 66% and 70% under the best preforming fixed configurations, with negligible additional time cost.

B. Generalization to Abstract Objects

Addressing the question of whether a reconfigurable gripper combined with soft fingers can effectively detect and grasp a variety of objects, the system was also tested on abstract shapes. The system's performance on abstract objects, as shown in Figure 20, further validates the benefits of reconfiguration. Each abstract object was designed to favor a specific grasp configuration. Fixed setups more often performed well when aligned with their corresponding object, failing more on others. However, the reconfigurable system consistently achieved high success by automatically adapting to the appropriate configuration. This demonstrates generalization capability, even for structurally diverse objects beyond natural shapes.

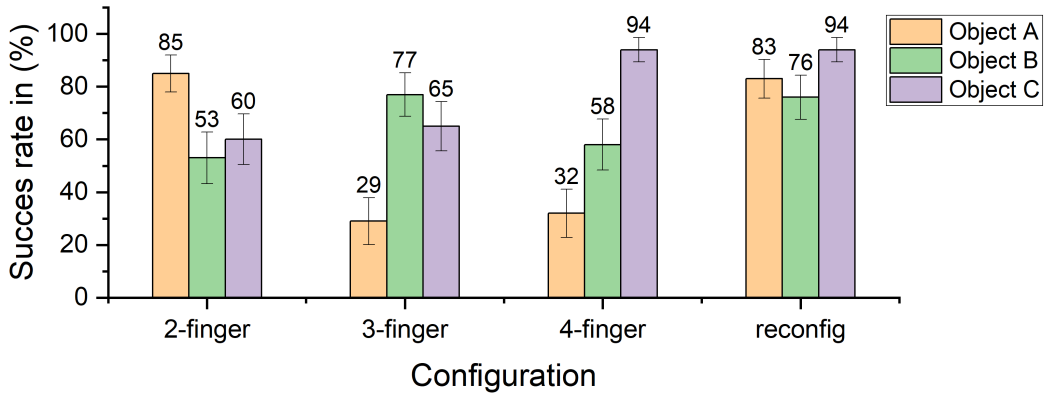

Fig. 20: Grasp success rates for abstract objects using various finger configurations. Each bar represents the percentage of successful grasps out of 100 trials with 95% confidence intervals.

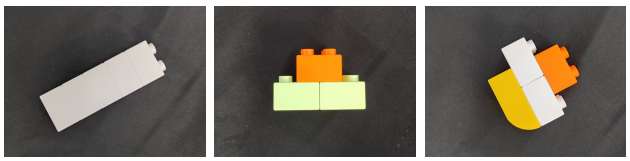

(a) Object-A (b) Object-B (c) Object-C

Fig. 21: Top view of abstract objects (Object A, B, and C) made from Duplo blocks, used for evaluating the robotic system.

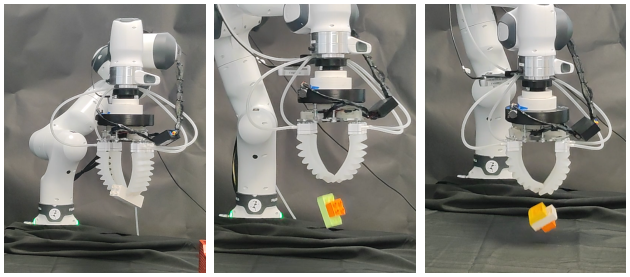

(a) Object A successful grasp (b) Object B failed grasp (c) Object C failed grasp

Fig. 22: Examples of 2-finger grasp attempts on abstract objects: one successful and two failed grasps.

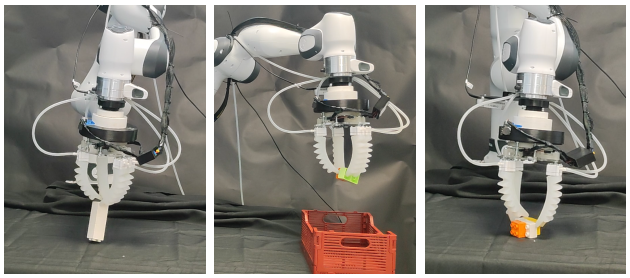

(a) Object A failed grasp (b) Object B successful grasp (c) Object C failed grasp

Fig. 23: Examples of 3-finger grasp attempts on abstract objects: one successful and two failed grasps.

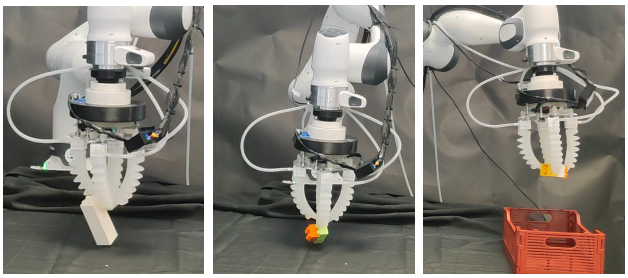

(a) Object A failed grasp (b) Object B failed grasp (c) Object C successful grasp

Fig. 24: Examples of 4-finger grasp attempts on abstract objects: one successful and two failed grasps.

C. Failure Analysis

Figures 17 through 24 illustrate both successful and failed grasp attempts using fixed finger configurations.

One frequent issue was misalignment, often resulting in the soft fingers colliding with the object rather than securely grasping it. This was especially prevalent in the 4-finger configuration, where the more spaced out configuration of fingers raised the likelihood of at least one finger colliding. The elongated shapes of objects like banana or Object A show this issue, as seen in Figure 19. A similar failure can be seen Figure 18, where the 3-finger configuration attempts to grasp an apple but ends up slamming into it due to poor alignment.

Another observed failure mode, particularly in the 2-finger configuration, was object tipping—where the object rolls or slips out of the gripper after initial contact. This occurred with both the banana and the apple. The banana's elongated and curved shape made it difficult to secure. Meanwhile, the apple's higher center of mass may have contributed to instability, causing it to rotate and fall during lifting.

For the 3-finger configuration, a common failure involved rotational slippage during the grasp attempt. In some trials, the object spun out of the grasp as the fingers closed unevenly or applied off-center force.

For the abstract objects, additional failure patterns were observed. In particular, Object A consistently failed to be grasped by the 3- and 4-finger configurations. This was primarily due to misalignment between the finger bending direction and the object's surface normal. Because Object A has smooth, flat surfaces, improper finger orientation led to poor contact. As a result, the fingers were unable to apply enough normal force to securely lift the object, often causing it to slip.

For Object B, its triangular and blocky shape introduced challenges in force distribution during a 4-finger grasp. The geometric features caused misalignment among the fingers, leading to uneven contact points and an imbalanced grasp force. This misalignment reduced the overall stability of the grasp, increasing the likelihood of failure.

D. Trade-Offs and Efficiency

The reconfigurable gripper introduces a small time overhead—approximately 3 seconds for reconfiguration within an average cycle time of 37 seconds. While not negligible, this delay is outweighed by the increase in grasp reliability. Similarly soft fingers present a trade-off between the applied gripping force and their non-intrusiveness. Their compliance can help improve this balance, but reduced force still lowers the likelihood of a successful grasp. Therefore, integrating a reconfigurable mechanism provides a valuable complement to soft fingers, enhancing adaptability and improving overall grasp success rates.

E. Practical Implications and Deployment Potential

This work demonstrates how robotic systems that integrate soft robotics and reconfigurable mechanisms can transition from controlled laboratory environments to real-world applications. By combining a reconfigurable gripper with soft robotic fingers and automating grasp selection using a YOLO-based object detection, this approach has strong potential for practical deployment in fields such as agriculture, logistics, and manufacturing. The integration of these components contributing to adaptability, and intelligent decision making forms a cohesive and functional system. Such synergy is essential for bridging the gap between academic research and real-world robotic solutions.

F. future work

Future work could focus on several areas to improve the performance of the robotic system. First, expanding the training dataset with a more diverse set of object types and geometries would allow for the development of more generalizable object detection models. Which could improve classification accuracy, particularly for unfamiliar objects.

Secondly, incorporating more advanced motion planning algorithms could enable the system to perform more complex tasks. Currently, the system relies on top-down grasps; future iterations could include side or angled approaches, allowing for manipulation in cluttered environments.

Finally, integrating high-level task planning could improve operational speed and enable the system to handle more complex tasks.

V. CONCLUSION

This paper addresses the challenge of reliably grasping diverse and fragile objects by integrating soft robotic fingers, a reconfigurable gripper, and a YOLOv11-OBB-based perception into a unified robotic platform. The soft fingers provide gentle, non-intrusive contact, while the reconfigurable gripper adapts to different shapes. Powered by deep learning vision using YOLOv11-OBB, the system autonomously picks the best grasp strategy for each object.

For this work a novel soft finger was designed, selected via FEM simulation, and validated through physical testing. YOLOv11-OBB was adapted in innovative manner not only to detect object location and orientation but also to infer the desired gripper configuration via class labels, enabling autonomous adjustment of grasp strategy. Making this system autonomous and versatile

Experimental evaluations on both natural (fruit) and abstract objects demonstrate that the proposed system significantly improves grasp success rates over fixed-configuration baselines—achieving up to 84.33% from 66% for abstract objects, and 84.67% from 70% for fruit, with only a modest increase in execution time.

These findings show that combining soft fingers, reconfigurable gripper with YOLO can enable practical, adaptable robotic systems suitable for real-world applications in agriculture and beyond.

REFERENCES

[1] R. Sparrow and M. Howard, "Robots in agriculture: prospects, impacts, ethics, and policy," *precision agriculture*, vol. 22, pp. 818–833, 2021.

[2] Z. Chunjiang, F. Beibei, L. Jin, and F. Qingchun, "Agricultural robots: Technology progress, challenges and trends," *Smart agriculture*, vol. 5, no. 4, p. 1, 2023.

[3] D. KUMAR, V. CHOUDHARY, N. KUMAR, B. JYOTI, S. MANDAL, P. JEET, P. K. SUNDARAM, and A. SINGH, "Robots for harvesting of horticultural crop: A review: Harvesting fruits by robots," *Journal of AgriSearch*, vol. 11, no. 3, pp. 152–164, 2024.

[4] F. Visentin, F. Castellini, and R. Muradore, "A soft, sensorized gripper for delicate harvesting of small fruits," *Computers and Electronics in Agriculture*, vol. 213, p. 108202, 2023.

[5] A. Gafer, D. Heymans, D. Prattichizzo, and G. Salvietti, "The quad-spatula gripper: A novel soft-rigid gripper for food handling," in *2020 3rd IEEE International Conference on Soft Robotics (RoboSoft)*. IEEE, 2020, pp. 39–45.

[6] O. Morikage, Z. Wang, and S. Hirai, "Multi-fingered soft gripper driven by bellows actuator for handling food materials," in *2021 27th International Conference on Mechatronics and Machine Vision in Practice (M2VIP)*. IEEE, 2021, pp. 363–368.

[7] J. F. Elfferich, E. Shahabi, C. Della Santina, and D. Dodou, "Berrytwist: A twisting-tube soft robotic gripper for blackberry harvesting," *IEEE Robotics and Automation Letters*, 2024.

[8] M. Baggetta, O. Pennacchio, S. Pirozzi, and G. Berselli, "A reconfigurable four-finger gripper for versatile application in the agri-food industry," *IEEE/ASME Transactions on Mechatronics*, 2025.

[9] P. Cheng, Y. Lu, C. Wu, and B. Yan, "Reconfigurable bionic soft pneumatic gripper for fruit handling based on shape and size adaptation," *Journal of Physics D: Applied Physics*, vol. 56, no. 4, p. 044003, 2022.

[10] L. Hashanjana, P. Senanayaka, I. Madushan, H. Himaruwan, A. L. Kulasekera, and P. C. Dassanayake, "Design and development of a soft gripper system for difficult-to-handle food items," in *2023 Moratuwa Engineering Research Conference (MERCon)*. IEEE, 2023, pp. 678–683.

[11] A. K. Mishra, E. Del Dottore, A. Sadeghi, A. Mondini, and B. Mazzolai, "Simba: Tendon-driven modular continuum arm with soft reconfigurable gripper," *Frontiers in Robotics and AI*, vol. 4, p. 4, 2017.

[12] P. M. Khin, C.-H. Yeow, and M. H. J. Ang, "Hyper-versatile gripping: Synergizing mechanical and machine intelligence of a hybrid robotic gripper," *Advanced Intelligent Systems*, vol. 6, no. 4, p. 2300533, 2024.

[13] J. H. Low, P. M. Khin, Q. Q. Han, H. Yao, Y. S. Teoh, Y. Zeng, S. Li, J. Liu, Z. Liu, P. V. y Alvarado *et al.*, "Sensorized reconfigurable soft robotic gripper system for automated food handling," *IEEE/ASME Transactions On Mechatronics*, vol. 27, no. 5, pp. 3232–3243, 2021.

[14] A. T. Mathew, I. Hussain, C. Stefanini, I. M. B. Hmida, and F. Renda, "Resoft gripper: A reconfigurable soft gripper with monolithic fingers and differential mechanism for versatile and delicate grasping," in *2021 IEEE 4th international conference on soft robotics (RoboSoft)*. IEEE, 2021, pp. 372–378.

[15] S. Vasudevan, M. L. Mekhalfi, C. Blanes, M. Lecca, F. Poiesi, P. I. Chippendale, P. M. Fresnillo, W. M. Mohammed, and J. L. M. Lastra, "Robotics and machine vision for primary food manipulation and packaging: A survey," *IEEE Access*, 2024.

[16] X. Zhu, F. Chen, Y. Zheng, C. Chen, and X. Peng, "Detection of camellia oleifera fruit maturity in orchards based on modified lightweight yolo," *Computers and Electronics in Agriculture*, vol. 226, p. 109471, 2024.

[17] Y. Chen, H. Xu, P. Chang, Y. Huang, F. Zhong, Q. Jia, L. Chen, H. Zhong, and S. Liu, "Ces-yolov8: Strawberry maturity detection based on the improved yolov8," *Agronomy*, vol. 14, no. 7, p. 1353, 2024.

[18] P. Jiang, D. Ergu, F. Liu, Y. Cai, and B. Ma, "A review of yolo algorithm developments," *Procedia computer science*, vol. 199, pp. 1066–1073, 2022.

[19] G. Udupa, P. Sreedharan, P. Sai Dinesh, and D. Kim, "Asymmetric bellow flexible pneumatic actuator for miniature robotic soft gripper," *Journal of Robotics*, vol. 2014, no. 1, p. 902625, 2014.

[20] B. Mosadegh, P. Polygerinos, C. Keplinger, S. Wennstedt, R. F. Shepherd, U. Gupta, J. Shim, K. Bertoldi, C. J. Walsh, and G. M. Whitesides, "Pneumatic networks for soft robotics that actuate rapidly," *Advanced functional materials*, vol. 24, no. 15, pp. 2163–2170, 2014.

[21] H. Li, H. Bai, Z. Wang, Y. Tan, and Y. Tang, "Soft bioinspired pneumatic actuator for adaptive grasping based on direct ink writing method," *Sensors and Actuators A: Physical*, vol. 367, p. 115041, 2024.

[22] M. Xu, H. Liu, D. Zhang, and L.-r. Su, "Corrugated v-fold soft actuator with large deformation and high force density," *Smart Materials and Structures*, vol. 32, no. 11, p. 115030, 2023.

[23] T. Hao, H. Xiao, J. Wang, X. Wang, S. Liu, and Q. Liu, "Friction enhancement through fingerprint-like soft surface textures in soft robotic grippers for grasping abilities," *Tribology Letters*, vol. 72, no. 2, p. 47, 2024.

[24] L. Marechal, P. Balland, L. Lindenroth, F. Petrou, C. Kontovounisios, and F. Bello, "Towards a common framework and database of materials for soft robotics," *Soft Robotics*, vol. 0, no. 0, p. null, 2020.

[25] G. Jocher, J. Qiu, and A. Chaurasia, "Ultralytics yolo," Ultralytics, if you use this software, please cite it using this metadata. [Online]. Available: https://ultralytics.com

APPENDIX

APPENDIX A: FSM DIAGRAM

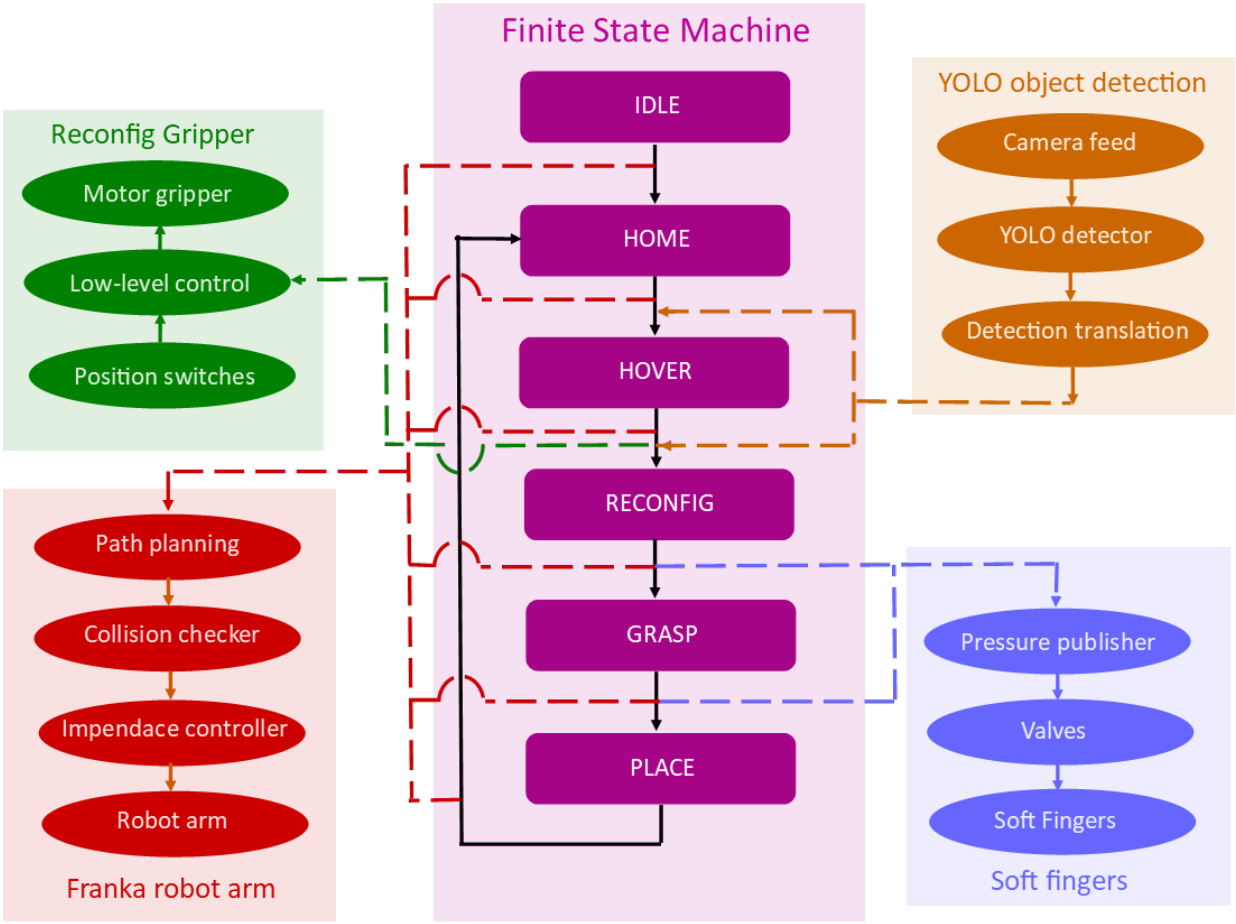

Fig. 25: Finite State Machine (FSM) diagram

APPENDIX B: PHYSICAL WIRING SCHEMATIC

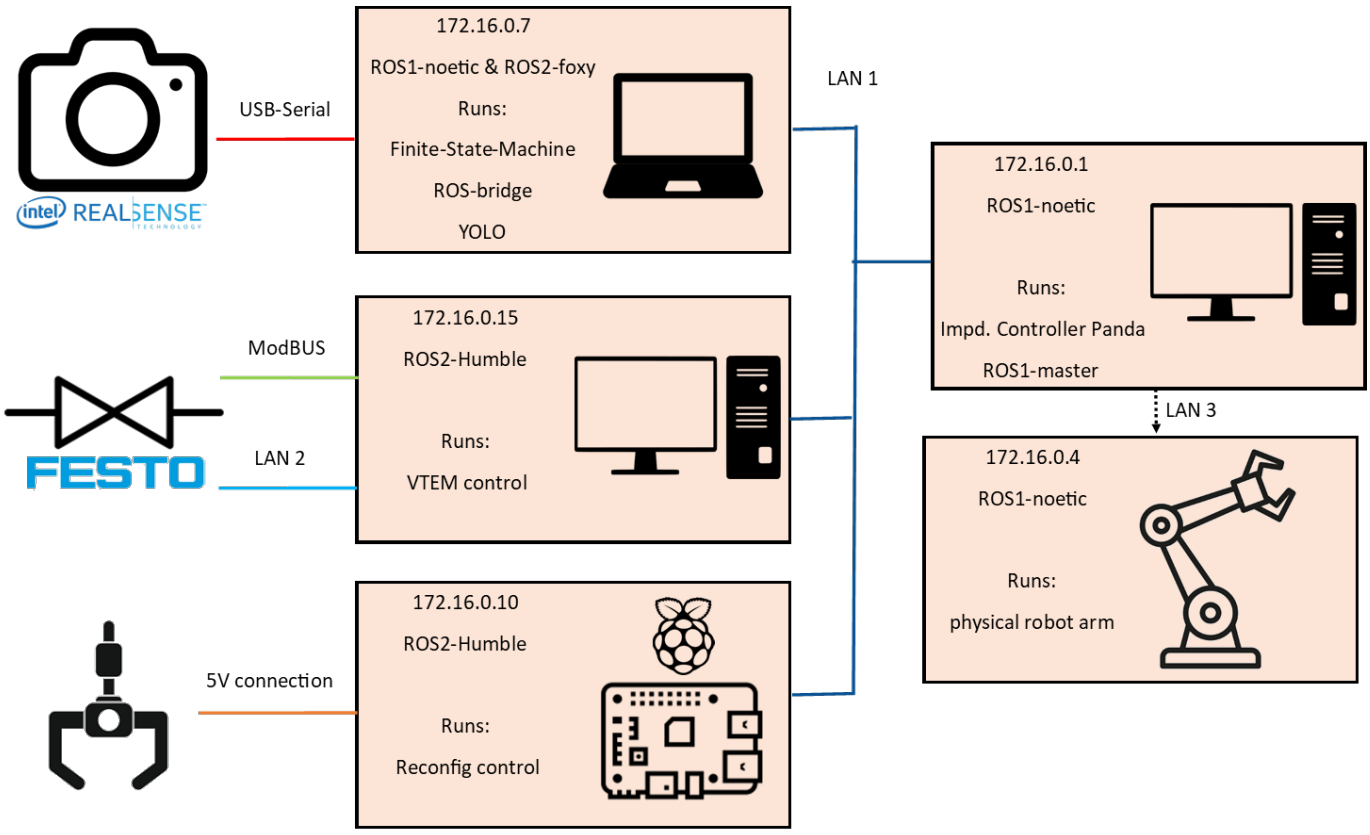

Fig. 26: Schematic of network setup

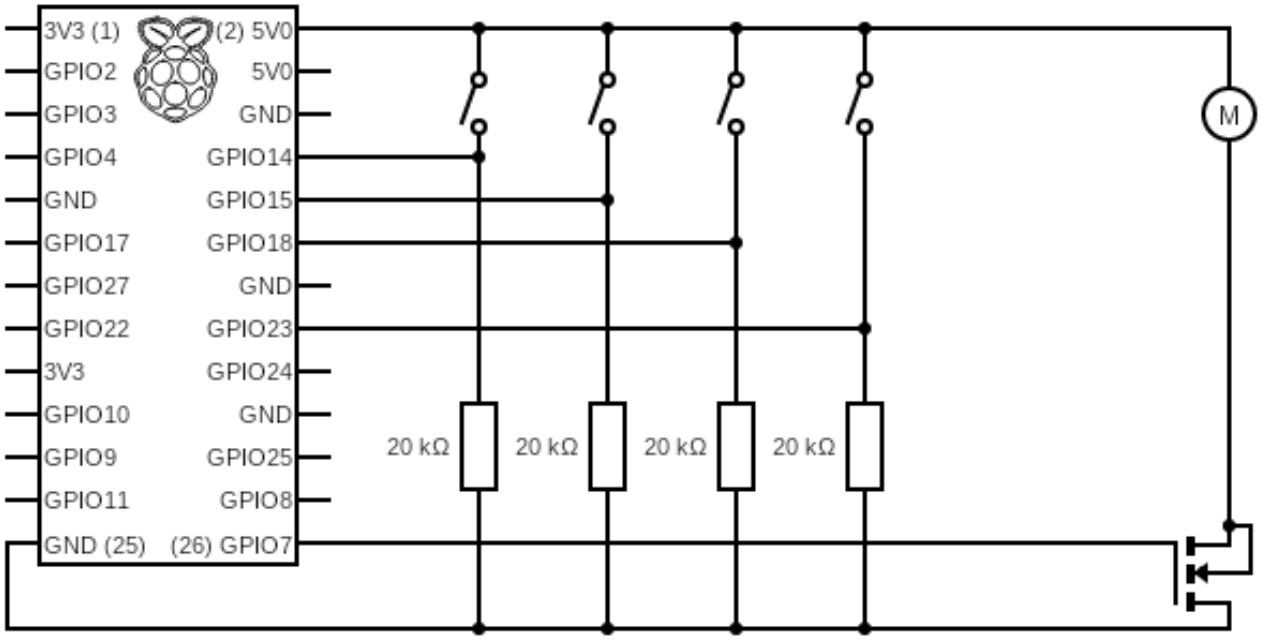

Fig. 27: Schematic of circuit wiring Reconfigurable gripper

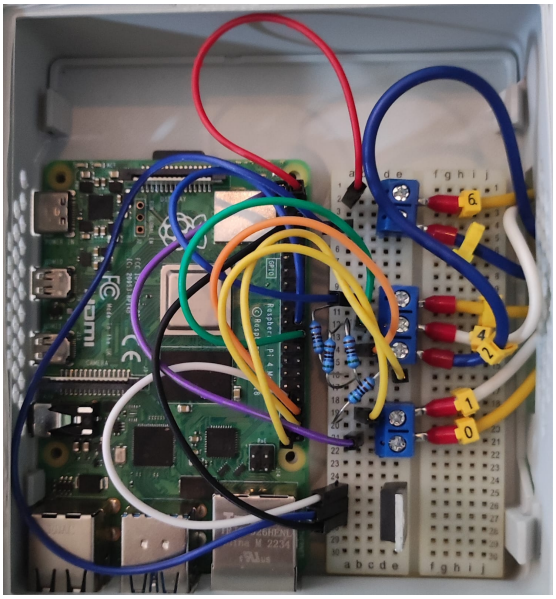

Fig. 28: Image circuit wiring Reconfigurable gripper

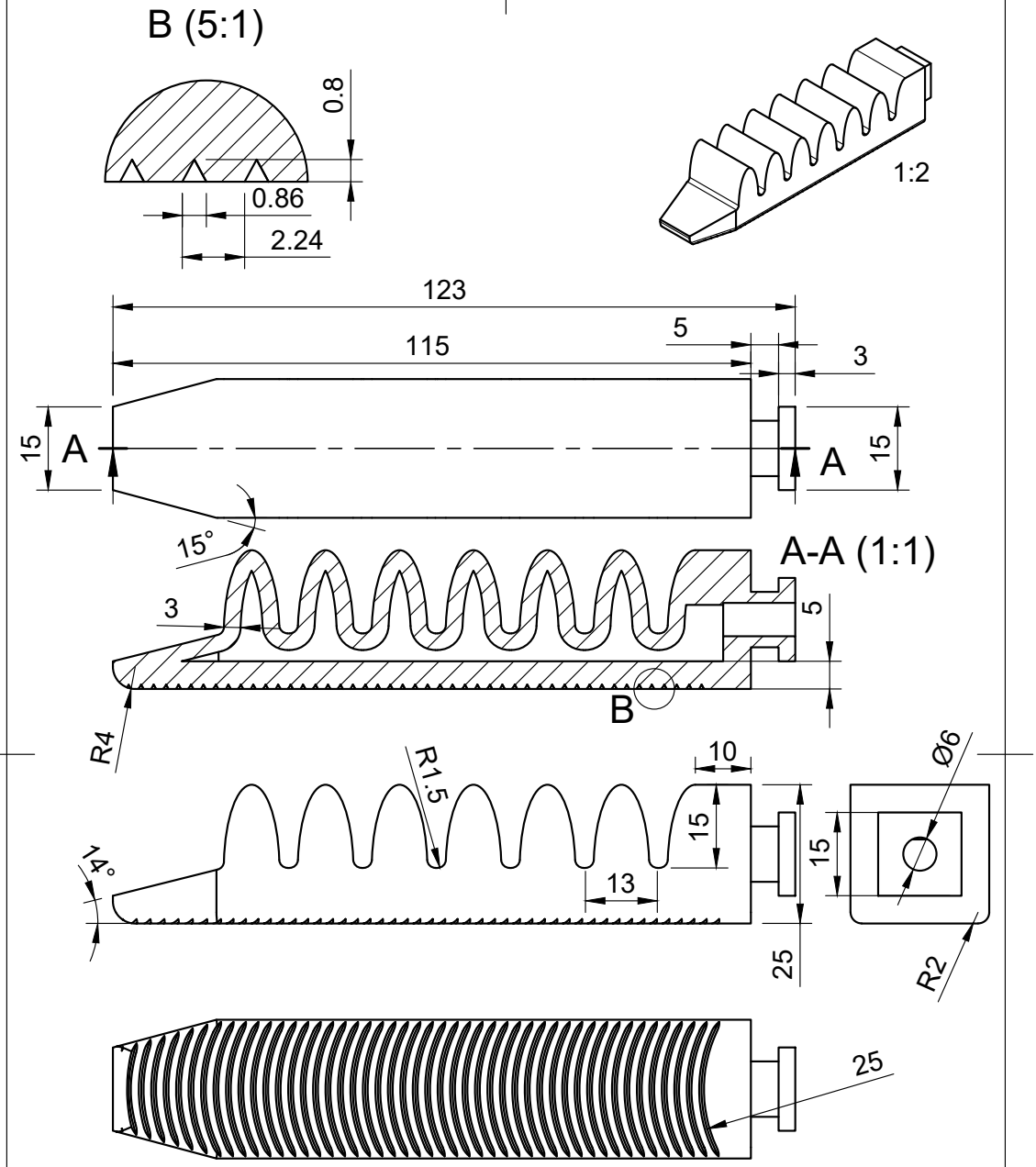

Part Name: FN35				All in mm
Notes:	Created by: Job Keijts		Date: 6-5-2025	
Material: Silicone Rubber		Scale: 1:1	Format: A4	Sheet: 1/1

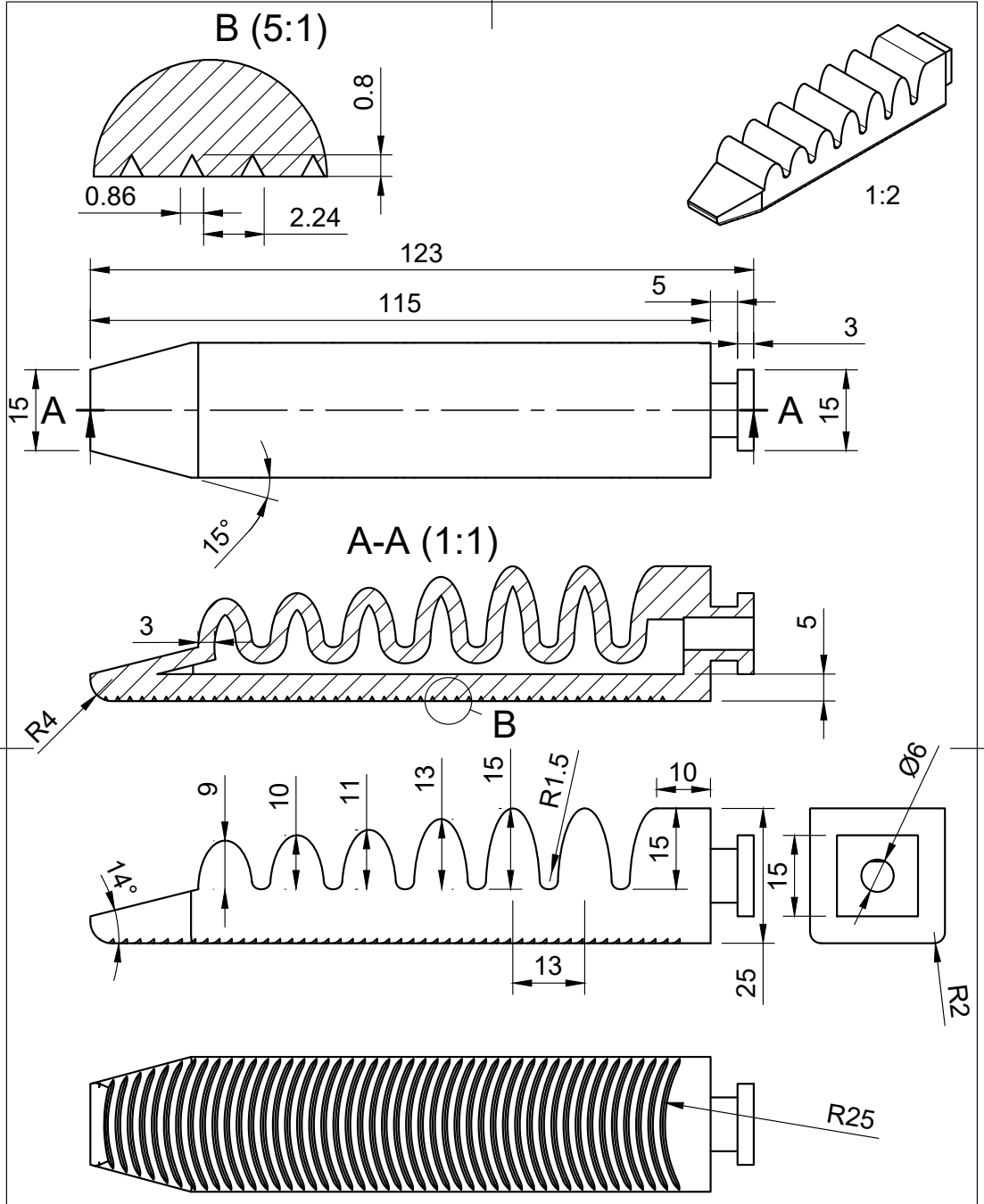

Part Name: FL35				All in mm
Notes:	Created by: Job Keijts		Date: 9-6-2025	
Material: Silicone Rubber		Scale: 1:1	Format: A4	Sheet: 1/1

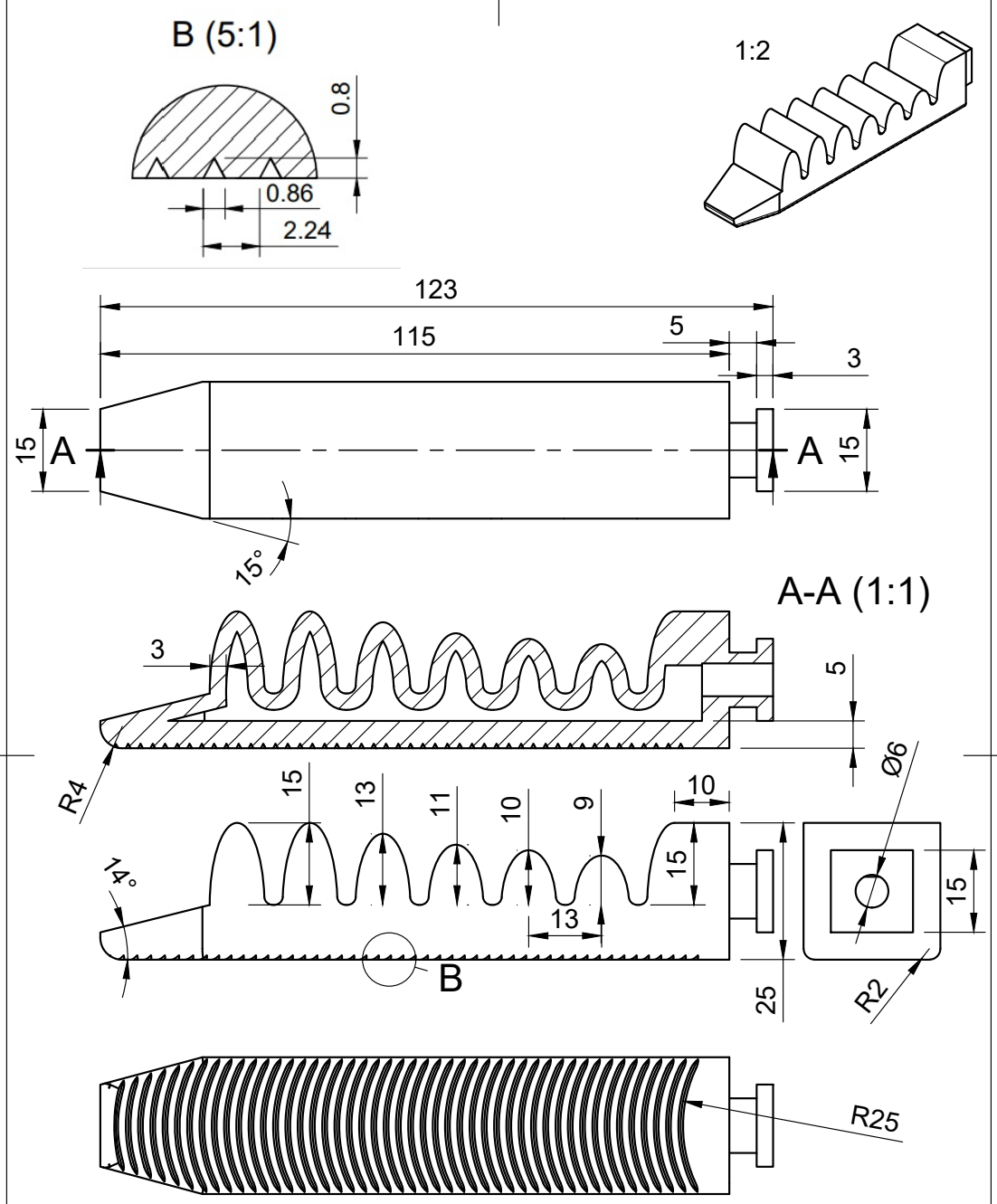

Part Name: FH35			All in mm	
Notes:	Created by: Job Keijts		Date: 1-6-2025	
Material: Silicone Rubber		Scale: 1:1	Format: A4	Sheet: 1/1

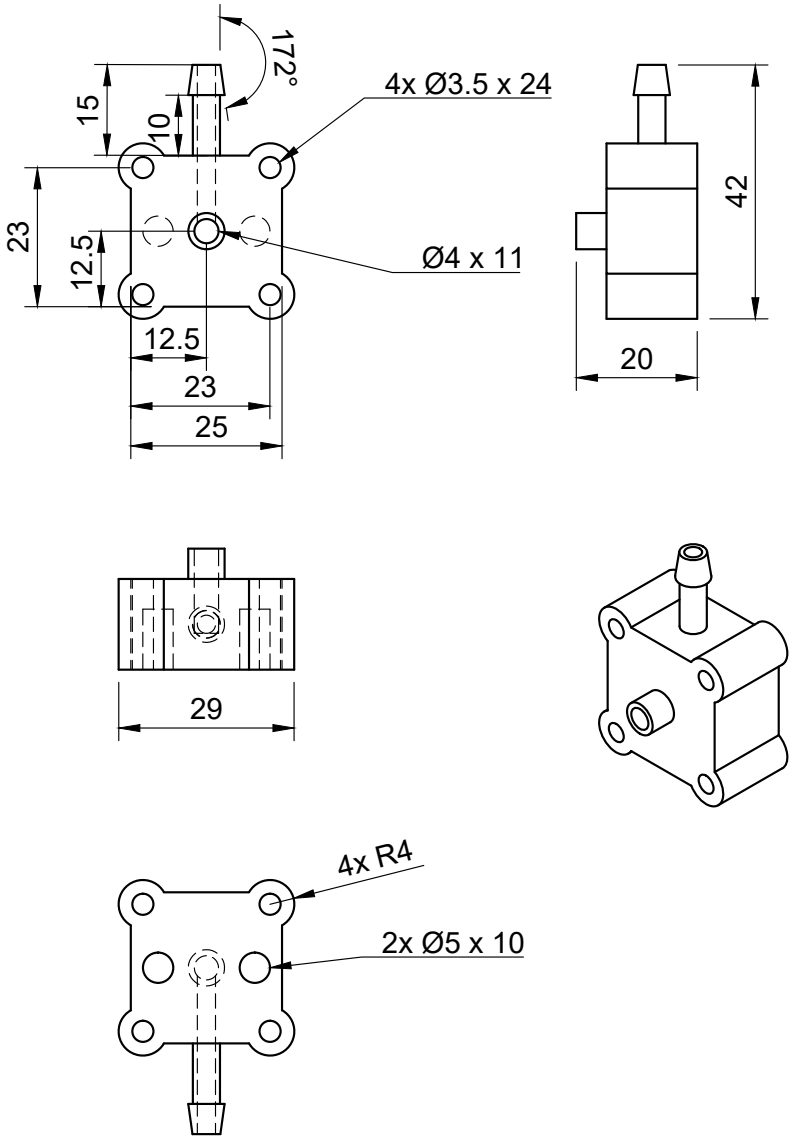

Part Name: Block				All in mm
Notes:		Created by: Job Keijts	Date: 2-6-2025	
Material: PLA		Scale: 1:1	Format: A4	Sheet: 1/1

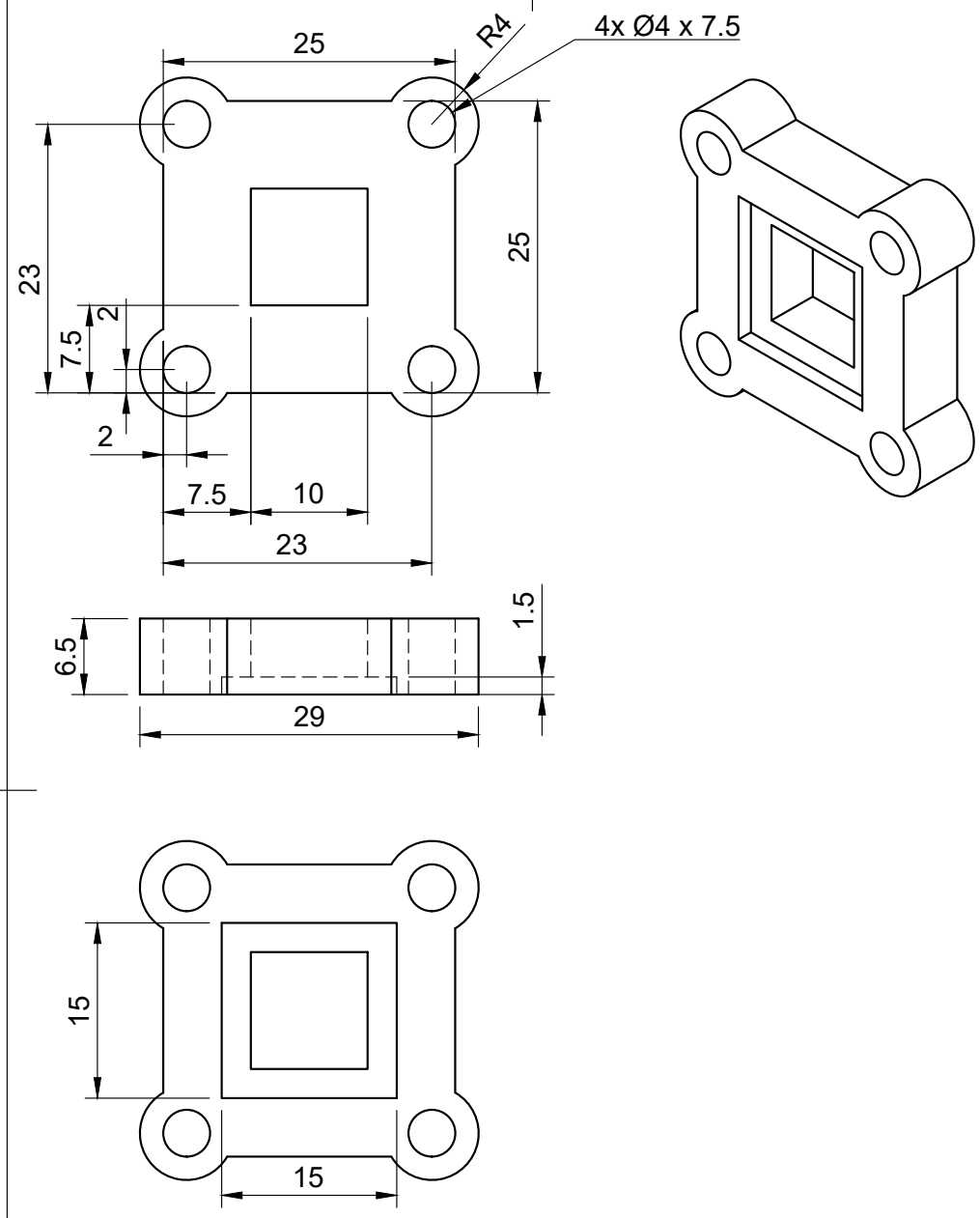

Part Name: Ring			All in mm
Notes:	Created by: Job Keijts	Date: 10-6-2025	
Material: PLA	Scale: 2:1	Format: A4	Sheet: 1/1

APPENDIX E: EXPERIMENT SETUP

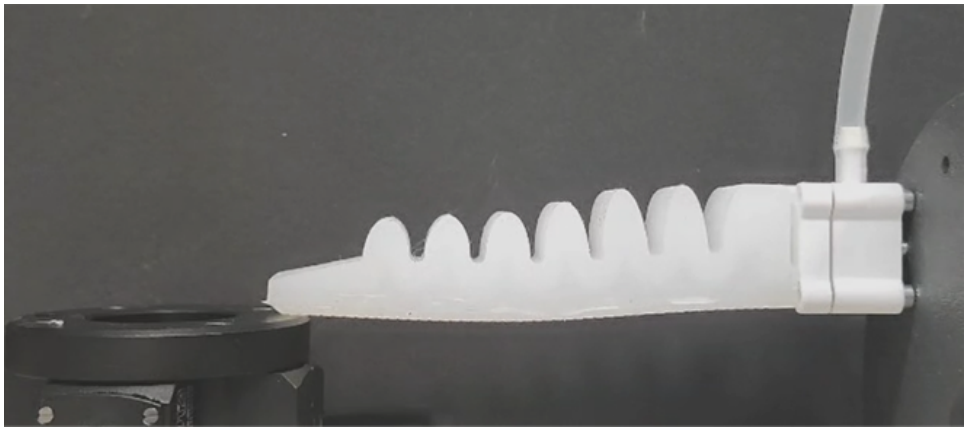

(a) Unpressurized

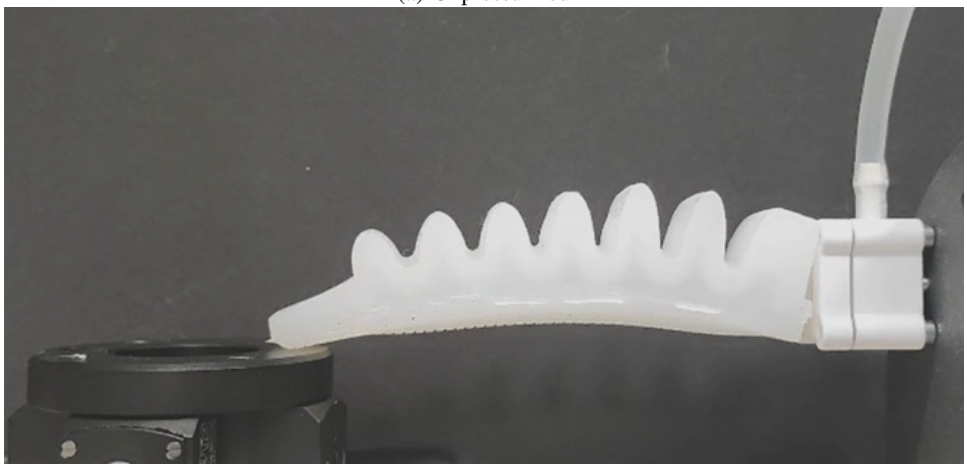

(b) Pressurized

Fig. 29: Experimental setup for force testing

(a) Wood surface

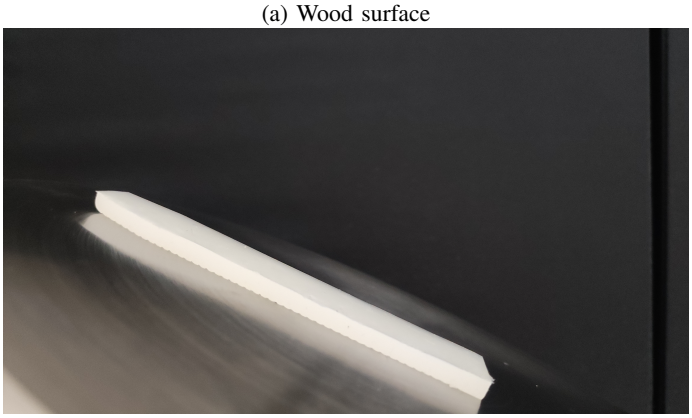

(b) Steel surface

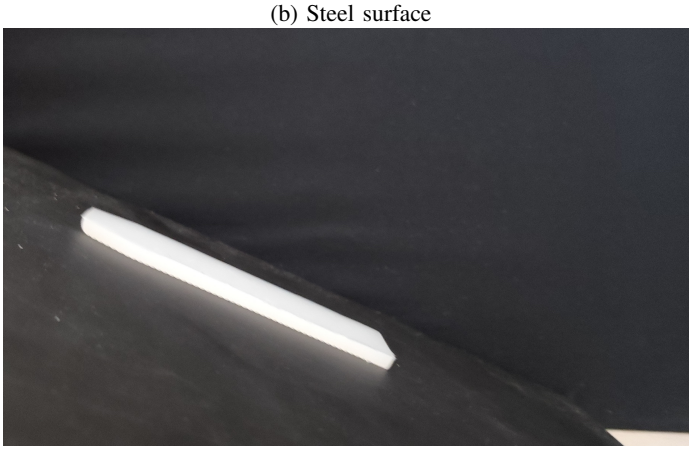

(c) PVC surface

Fig. 30: Experimental setup for friction testing on different surfaces

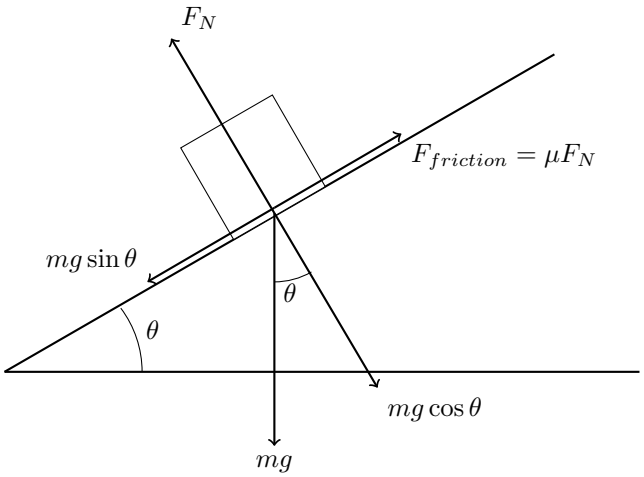

$$\mu = \frac{F_friction}{F_N} = \frac{mg \sin\theta}{mg \cos\theta} = \tan\theta$$

Fig. 31: Free body diagram of Test setup for friction

APPENDIX F: FEM PLOTS AND COMPARISONS

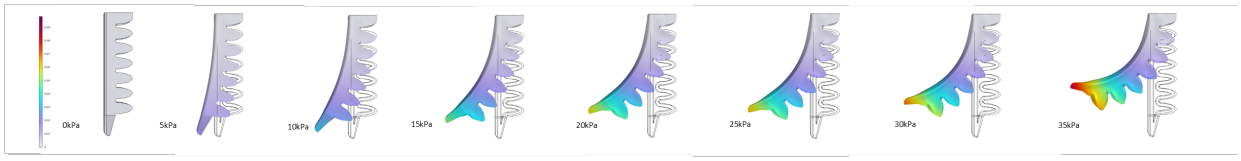

(a) FEM result: FN-model finger

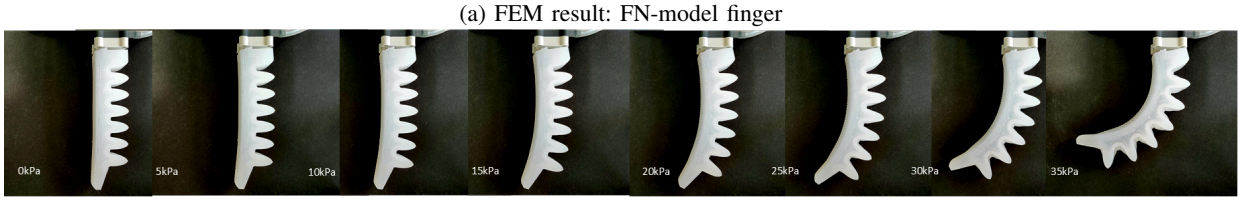

(b) Measurement: FN-model finger

Fig. 32: Comparison between FEM and measurements for FN-model finger

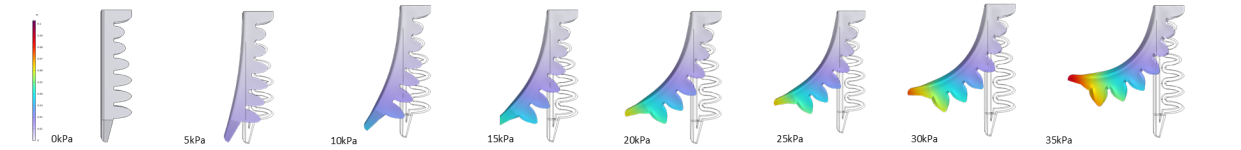

(a) FEM result: FH-model finger

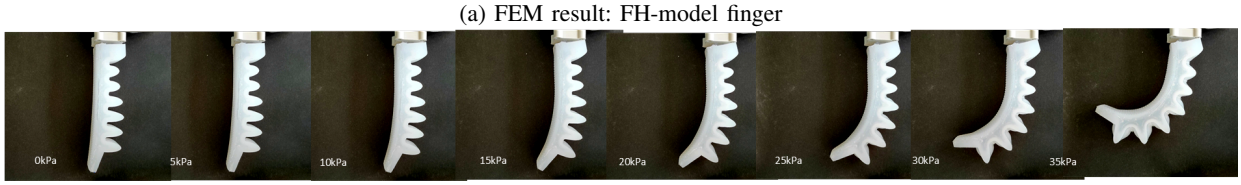

(b) Measurement: FH-model finger

Fig. 33: Comparison between FEM and measurements for FH-model finger

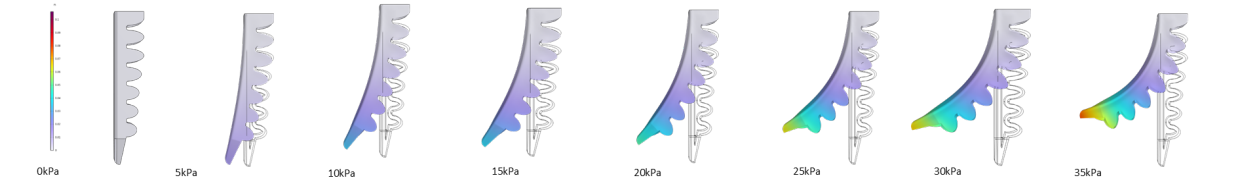

(a) FEM result: FL-model finger

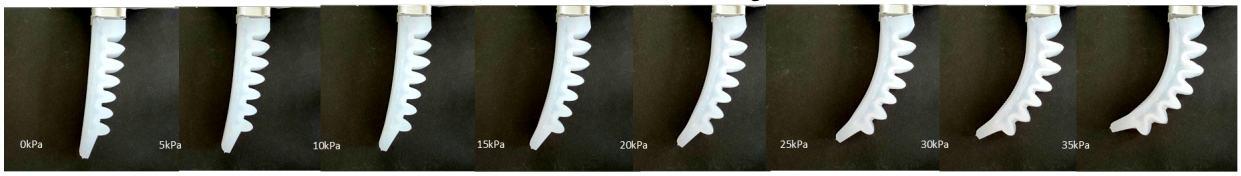

(b) Measurement: FL-model finger

Fig. 34: Comparison between FEM and measurements for FL-model finger

APPENDIX G: FEM VS EXPERIMENTAL FORCE RESULTS

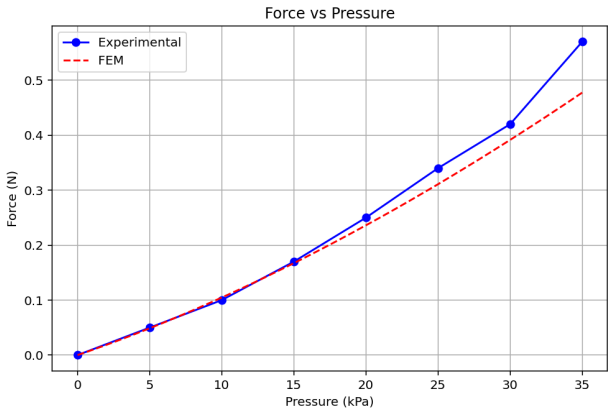

Fig. 35: Force: FEM vs experiment for FH-model

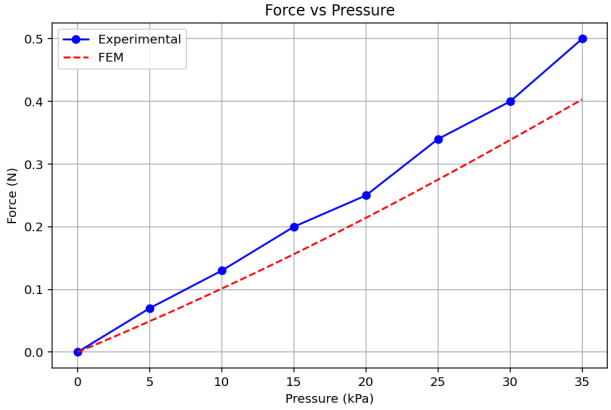

Fig. 36: Force: FEM vs experiment for FN-model

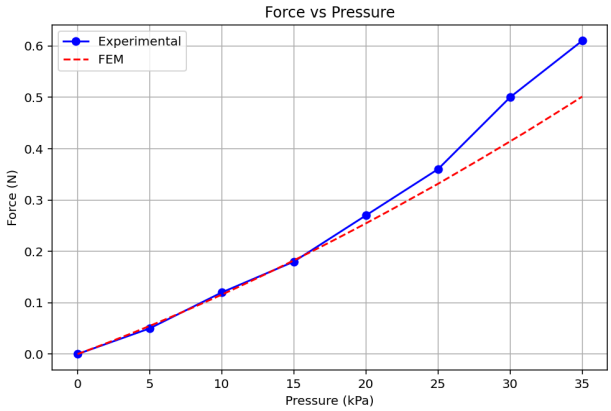

Fig. 37: Force: FEM vs experiment for FL-model

APPENDIX H: 3D-PLOT OF TOUCHABLE RANGE

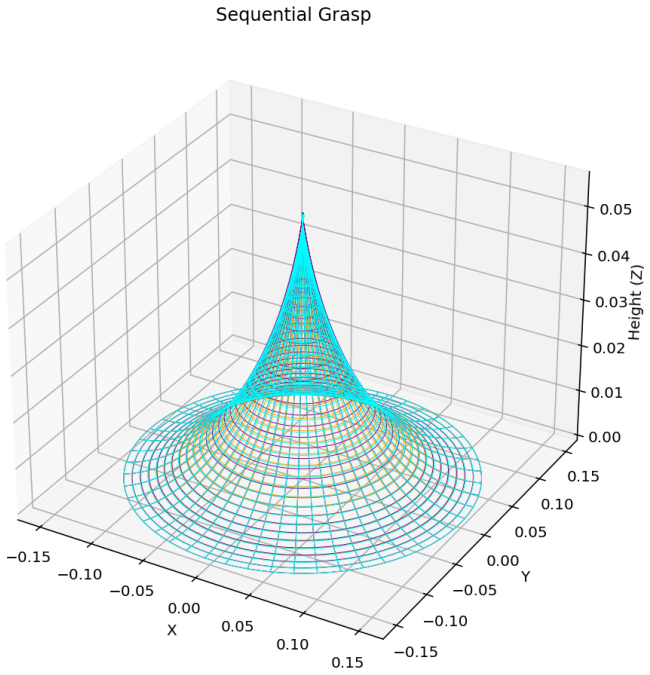

Fig. 38: 3d-representation of touchable range sequential grasp

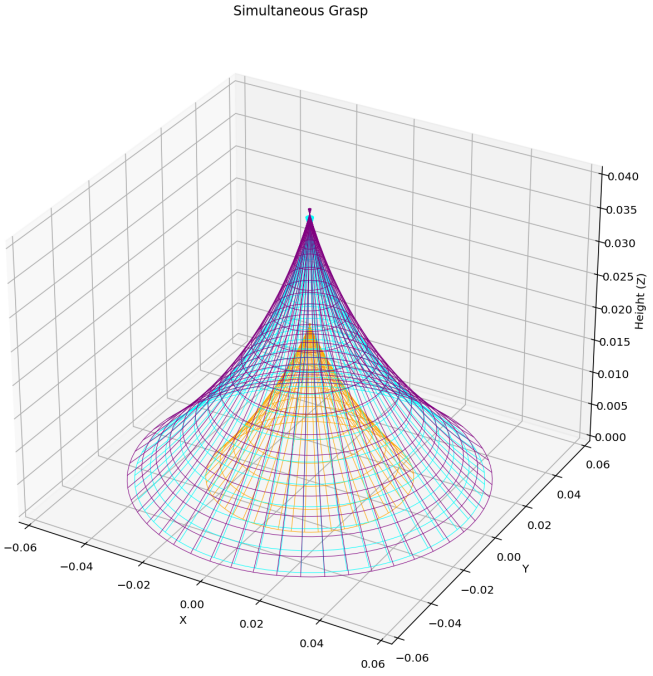

Fig. 39: 3d-representation of touchable range simultaneous grasp

APPENDIX I: EXAMPLES YOLO-DATSETS

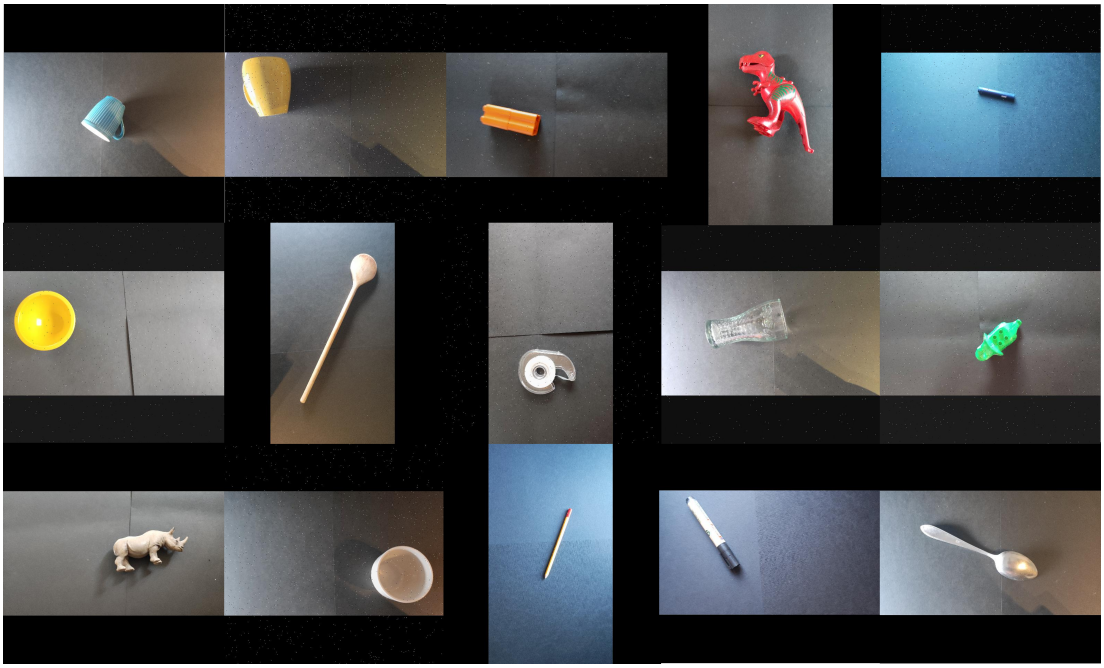

Fig. 40: Examples of Train Dataset colored images

Fig. 41: Examples of Test Dataset seen objects

Fig. 42: Examples of Test Dataset unseen objects

APPENDIX J: PR-PLOTS YOLO

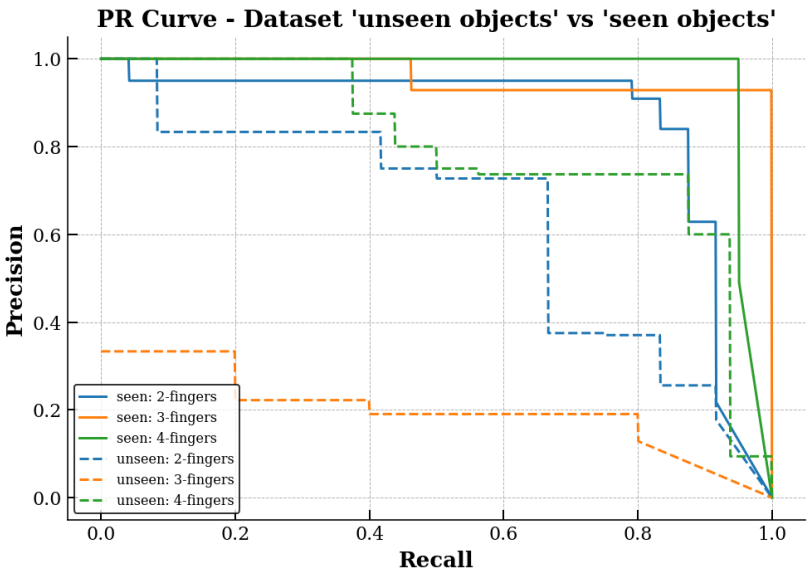

Fig. 43: Precision Recall curve YOLO-nano-color model with IoU=0.9

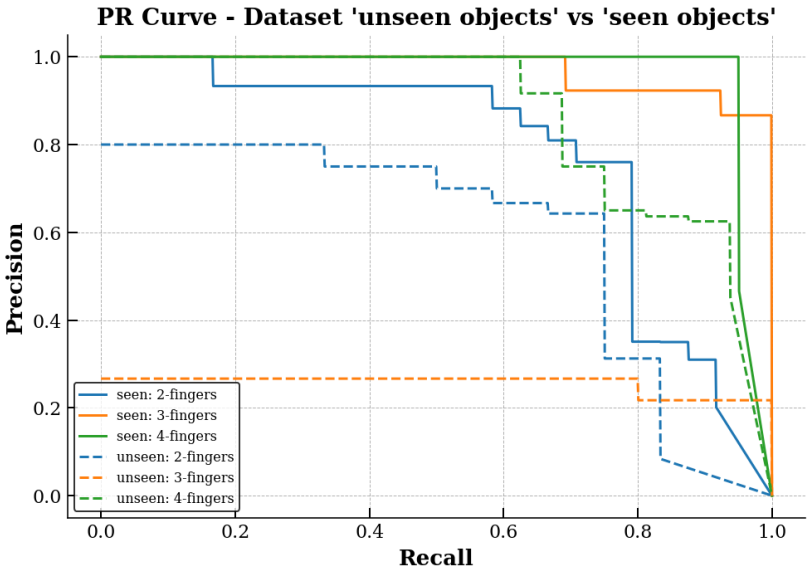

Fig. 44: Precision Recall curve YOLO-small-color model with IoU=0.9

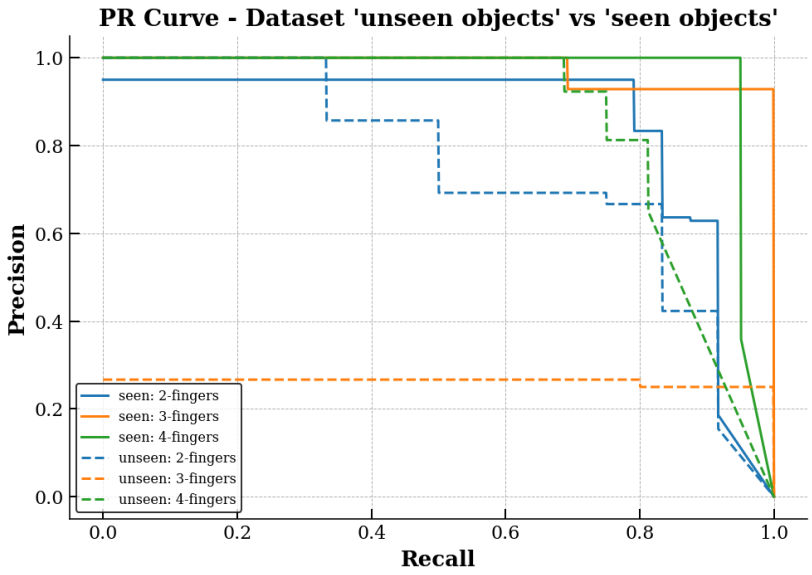

Fig. 45: Precision Recall curve YOLO-nano-grey model with IoU=0.9

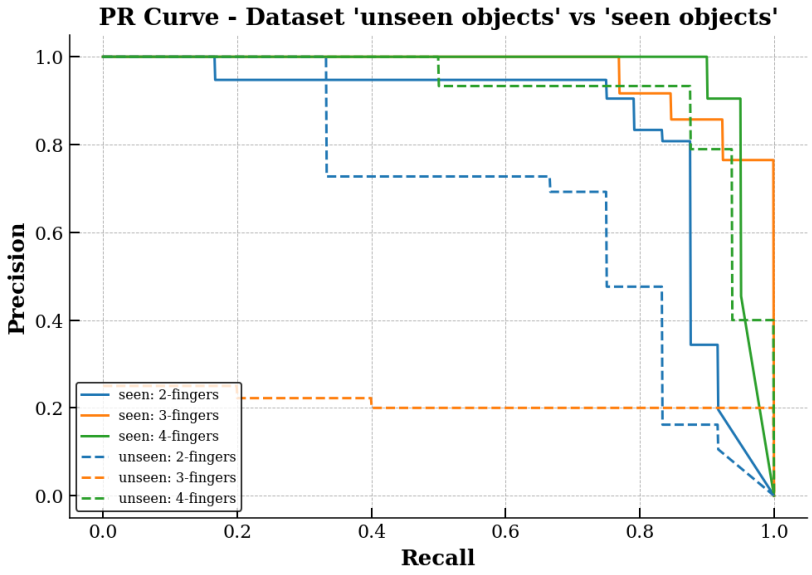

Fig. 46: Precision Recall curve YOLO-small-grey model with IoU=0.9

APPENDIX K: EXAMPLES DETECTIONS YOLO

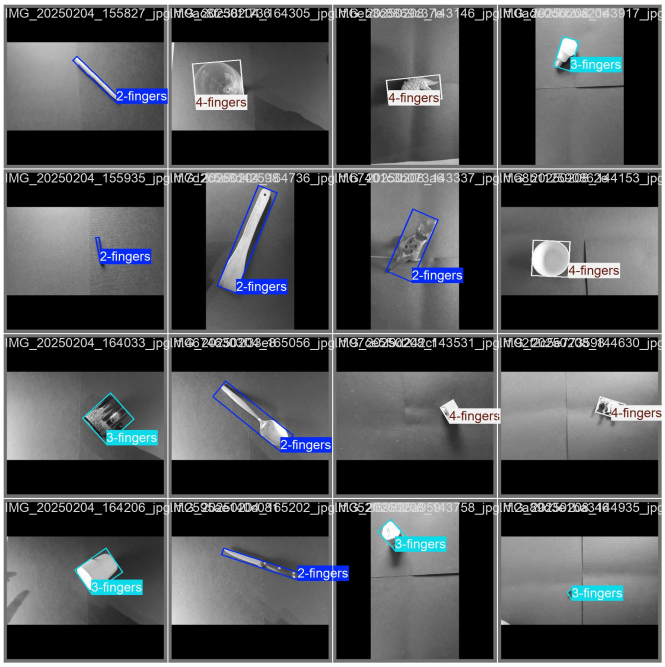

(a) Ground truth labels

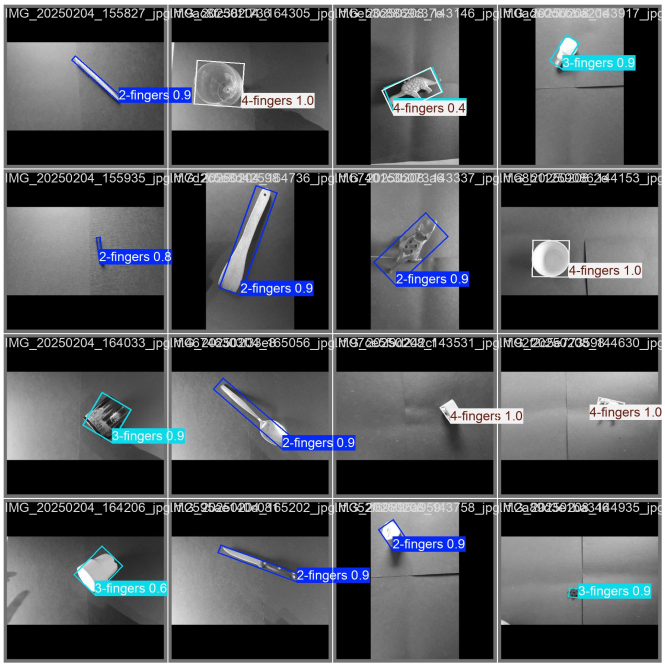

(b) Predictions

Fig. 47: YOLO-Nano-Grey results on seen objects with unseen images

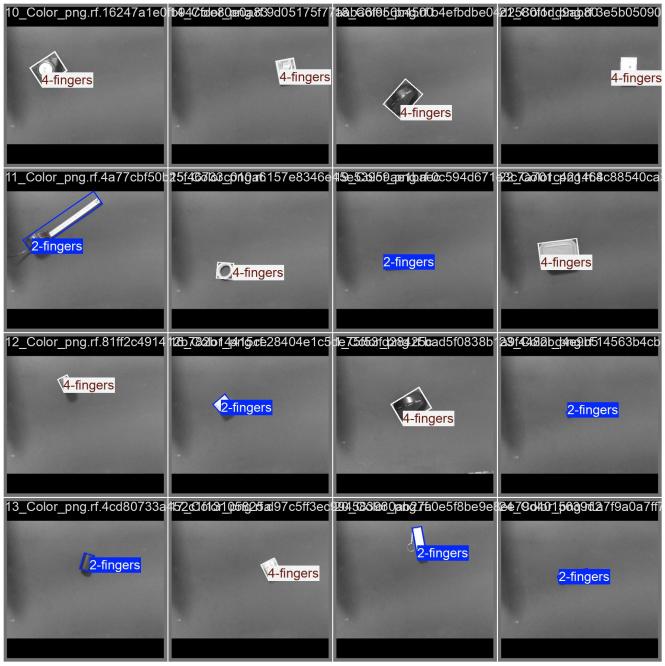

(a) Ground truth labels

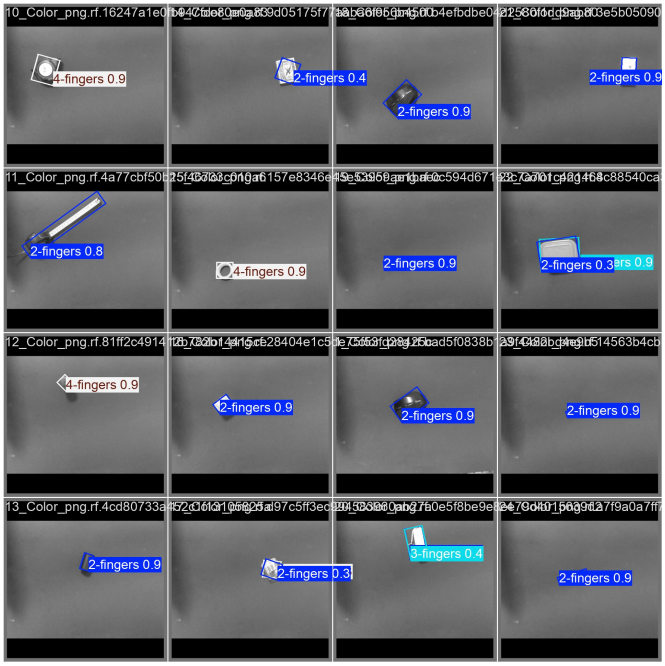

(b) Predictions

Fig. 48: YOLO-Nano-Grey results on unseen objects with unseen images

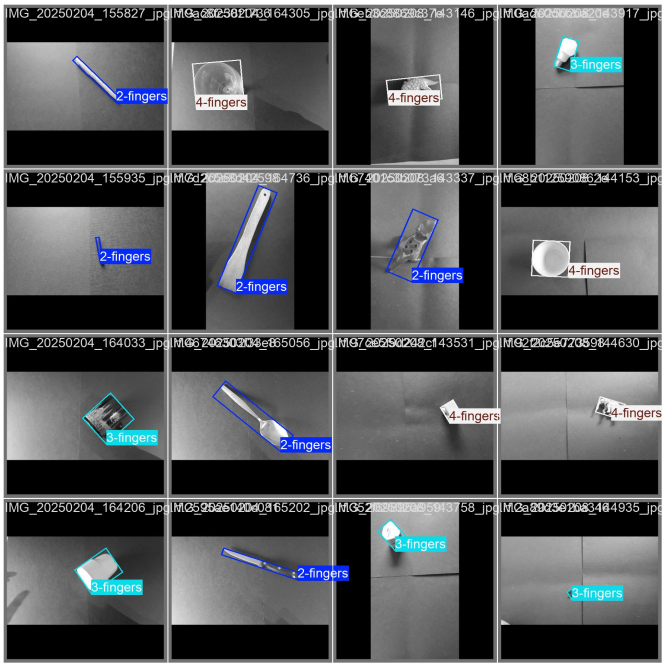

(a) Ground truth labels

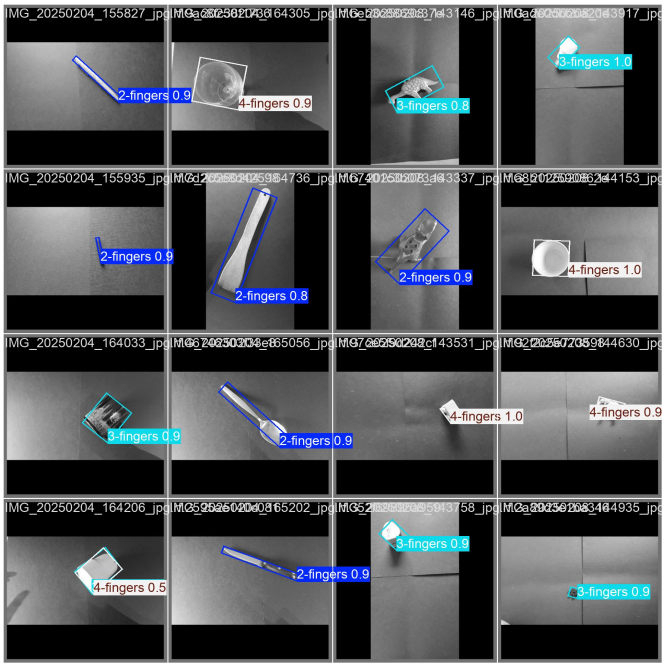

(b) Predictions

Fig. 49: YOLO-Small-Grey results on seen objects with unseen images

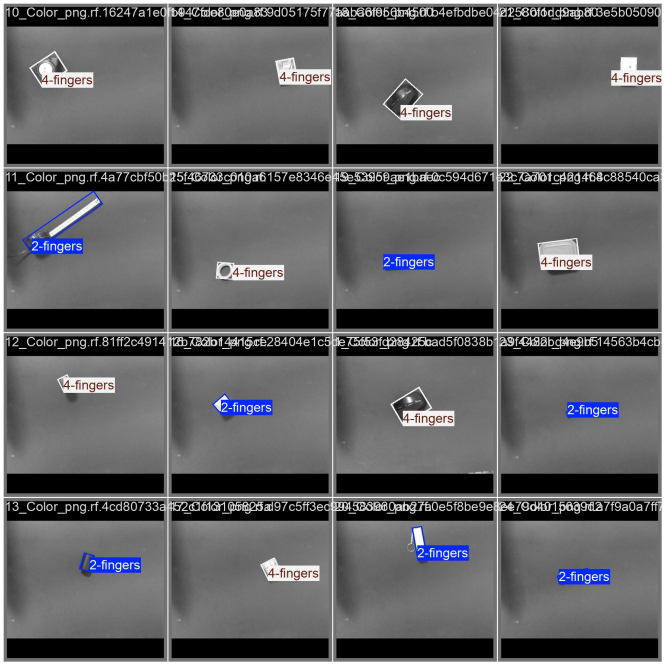

(a) Ground truth labels

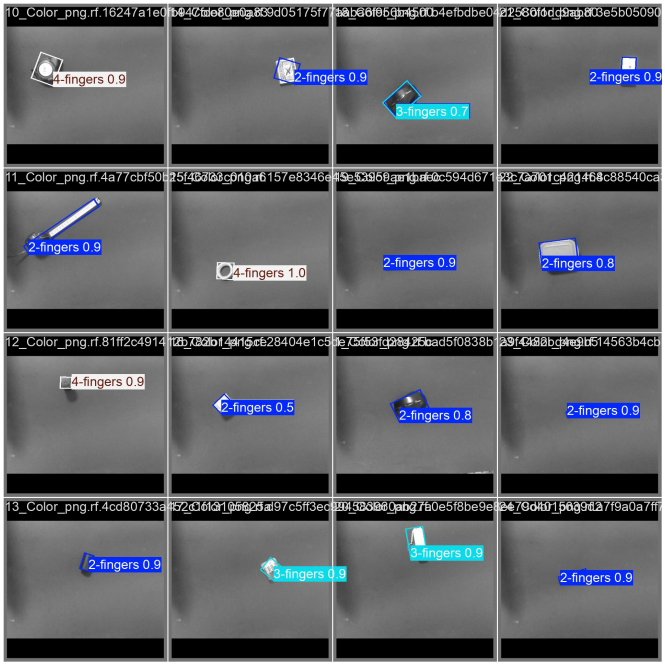

(b) Predictions

Fig. 50: YOLO-Small-Grey results on unseen objects with unseen images

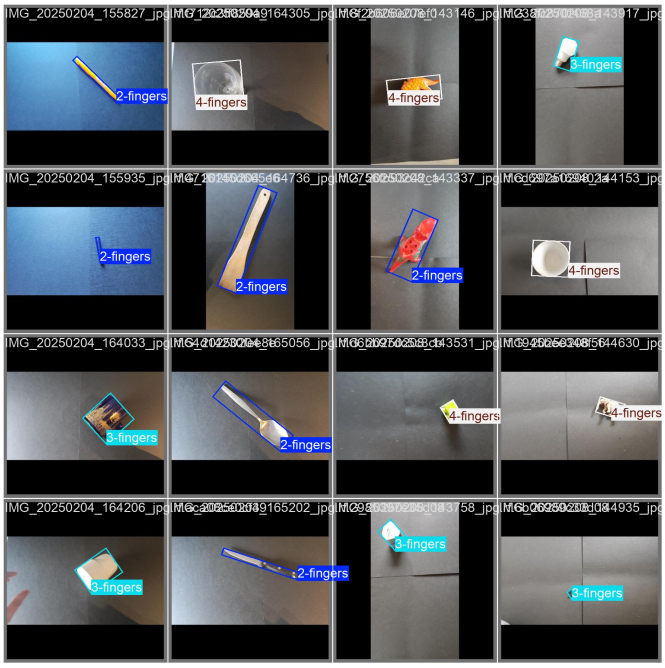

(a) Ground truth labels

(b) Predictions

Fig. 51: YOLO-Nano-Color results on seen objects with unseen images

(a) Ground truth labels

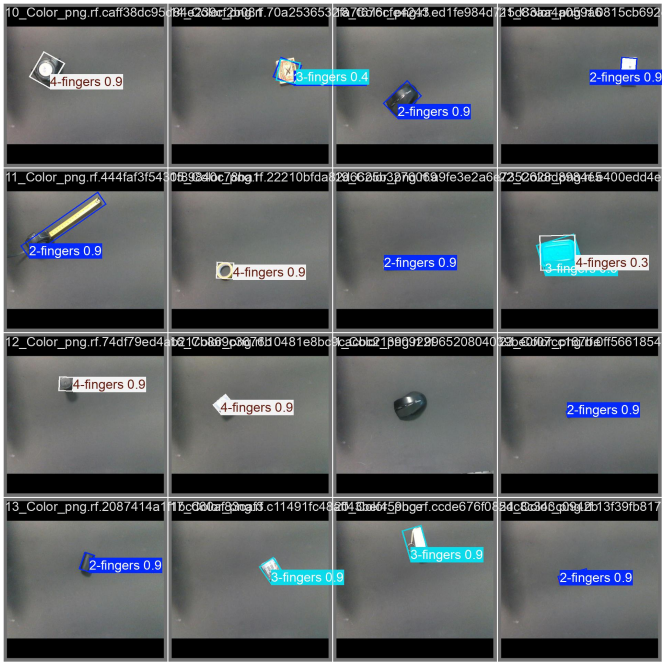

(b) Predictions

Fig. 52: YOLO-Nano-Color results on unseen objects with unseen images

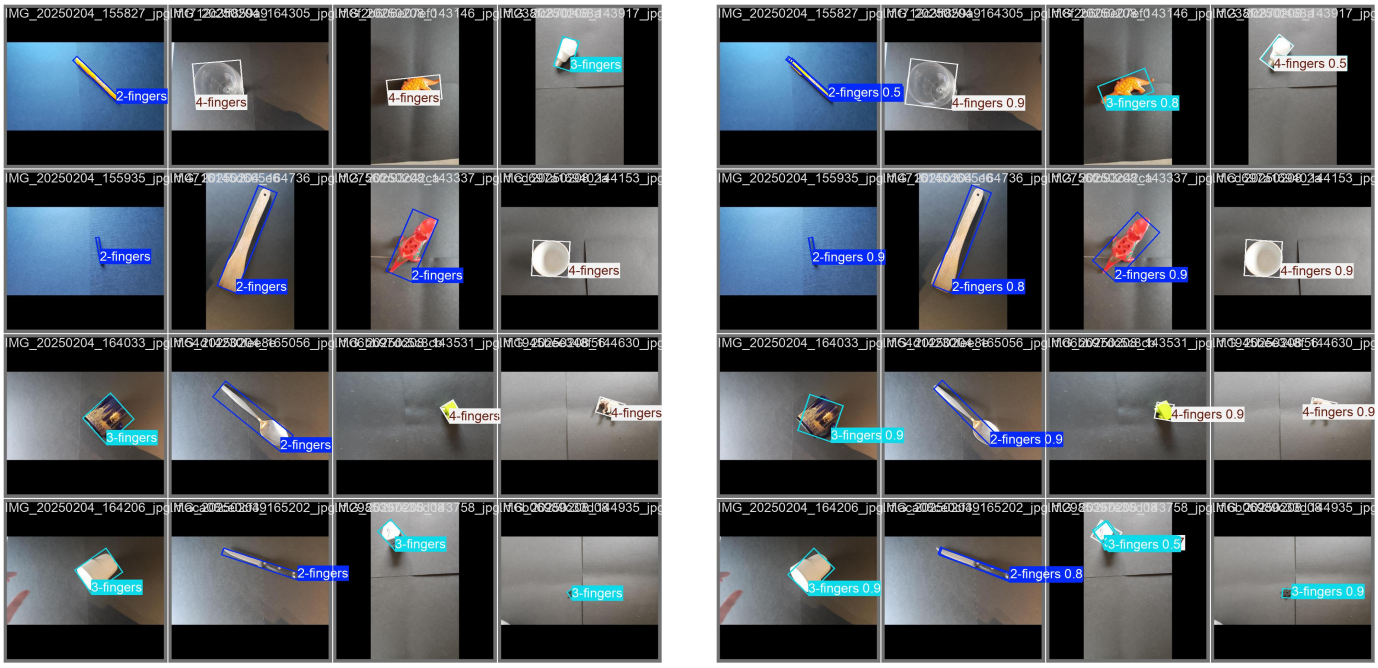

(a) Ground truth labels (b) Predictions

Fig. 53: YOLO-Small-Color results on seen objects with unseen images

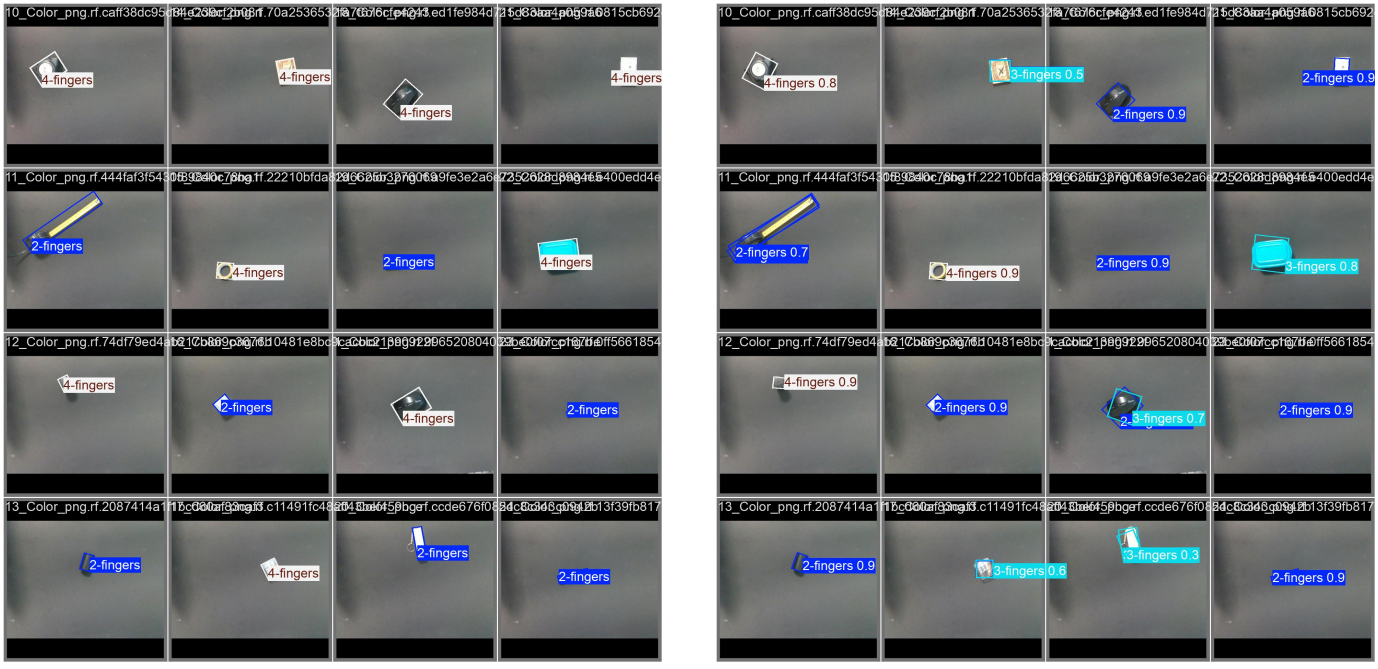

(a) Ground truth labels (b) Predictions

Fig. 54: YOLO-Small-Color results on unseen objects with unseen images